

Dust in the Local Interstellar Wind

April 26, 2024

Priscilla C. Frisch

Department of Astronomy and Astrophysics, University of Chicago, Chicago, IL 60637

Johann M. Dorschner

Astrophysikalisches Institut und Universitaets-Sternwarte, Schillergaesschen 3, D-07745

Jena, Germany

Johannes Geiss

International Space Science Institut, Bern, Switzerland

J. Mayo Greenberg

Leiden Observatory Laboratory, Postbus 9504, 2300 RA Leiden, The Netherlands

Eberhard Grün and Markus Landgraf

Max-Planck Institut fuer Kernphysik, Heidelberg, Germany

Peter Hoppe

Max-Planck-Institut for Chemistry, Cosmochemistry Department, P.O. Box 3060, D-55020

Mainz, Germany

Anthony P. Jones

Institut d'Astrophysique Spatiale, Université Paris XI, Bâtiment 121, 91405 Orsay Cedex,

France

Wolfgang Krätschmer

Max-Planck Institut fuer Kernphysik, Heidelberg, Germany

Timur J. Linde

University of Michigan, Aerospace Engineering, Ann Arbor, MI 48109

Gregor E. Morfill

Max-Planck-Institut fuer extraterrestrische Physik, 85740 Garching, Germany

William T. Reach

Infrared Processing and Analysis Center, California Institute of Technology, Mail Stop
100-22, Pasadena, CA 91125

Jonathan D. Slavin^{1,2}

Eureka Scientific Inc., 2452 Delmer St. Suite 100, Oakland, CA 94602-3017

Jiri Svestka

Prague Observatory, Prague, 11846 Czech Republic

Adolf N. Witt

Ritter Astrophysical Research Center, University of Toledo, Toledo, OH 43606

and

Gary P. Zank

Bartol Research Institute, University of Delaware, Newark, DE 19716

Received 8 October 1998; accepted 23 April 1999

¹Currently at the Department of Astronomy and Astrophysics, University of Chicago, Chicago, IL 60637

¹Also: University of California, Space Sciences Laboratory, Berkeley, CA 94720

²Postal address: NASA/Ames Research Center, MS 245-3, Moffett Field, CA 94035-1000

ABSTRACT

The gas-to-dust mass ratios found for interstellar dust within the Solar System, versus values determined astronomically for the cloud around the Solar System, suggest that large and small interstellar grains have separate histories, and that large interstellar grains preferentially detected by spacecraft are not formed exclusively by mass exchange with nearby interstellar gas. Observations by the Ulysses and Galileo satellites of the mass spectrum and flux rate of interstellar dust within the heliosphere are combined with information about the density, composition, and relative flow speed and direction of interstellar gas in the cloud surrounding the solar system to derive an *in situ* value for the gas-to-dust mass ratio, $R_{g/d}=94^{+46}_{-38}$. This ratio is dominated by the larger near-micron sized grains. Including an estimate for the mass of smaller grains, which do not penetrate the heliosphere due to charged grain interactions with heliosheath and solar wind plasmas, and including estimates for the mass of the larger population of interstellar micrometeorites, the total gas-to-dust mass ratio in the cloud surrounding the Solar System is half this value. Based on *in situ* data, interstellar dust grains in the of 10^{-14} to 10^{-13} g mass range are underabundant in the Solar System, compared to an MRN mass distribution scaled to the local interstellar gas density, because such small grains do not penetrate the heliosphere. The gas-to-dust mass ratios are also derived by combining spectroscopic observations of the gas-phase abundances in the nearest interstellar clouds. Measurements of interstellar absorption lines formed in the cloud around the solar system, as seen in the direction of ϵ CMa, give $R_{g/d}=427^{+72}_{-207}$ for assumed solar reference abundances, and $R_{g/d}=551^{+61}_{-251}$ for assumed B-star reference abundances. These values exceed the *in situ* value, suggesting either grain mixing or grain histories are not correctly understood,

or that sweptup stardust is present. Such high values for diffuse interstellar clouds are strongly supported by diffuse cloud data seen towards λ Sco and 23 Ori, provided B-star reference abundances apply. If solar reference abundances prevail, however, the surrounding cloud is seen to have greater than normal dust destruction compared to higher column density diffuse clouds. The cloud surrounding the Solar System exhibits enhanced gas-phase abundances of refractory elements such as Fe^+ and Mg^+ , indicating the destruction of dust grains by shock fronts. The good correlation locally between Fe^+ and Mg^+ indicates that the gas-phase abundances of these elements are dominated by grain destruction, while the poor correlation between Fe^+ and H° indicates either variable gas ionization or the decoupling of neutral gas and dust over parsec scalelengths. These abundances, combined with grain destruction models, indicate that the nearest interstellar material has been shocked with shocks of velocity $\sim 150 \text{ km s}^{-1}$. If solar reference abundances are correct, the low $R_{\text{g/d}}$ value towards λ Sco may indicate that at least one cloud component in this direction contains dust grains which have retained their silicate mantles, and are responsible for the polarization of the light from nearby stars seen in this general region. Weak frictional coupling between gas and dust in nearby low density gas permit inhomogeneities to be present.

Subject headings: Interplanetary medium — ISM: dust— ISM: abundances — solar system: general

1. Introduction

The direct detection of interstellar dust grains within the solar system by the Ulysses and Galileo satellites provides an opportunity to constrain the properties, history, and origin of these grains by comparing *in situ* and remote data. The *in situ* satellite data sample the large end of the grain size distribution, $0.1 \leq a_{\text{gr}} \leq \sim 4 \mu\text{m}$ (a_{gr} is grain radius), since small grains are excluded from the inner heliosphere by interaction with the solar wind and in the heliopause region (Levy and Jokipii 1976, Wallis 1987, Kimura and Mann 1998, §3). In contrast, optical and ultraviolet observations of extinction and polarization of starlight by interstellar dust grains give information on dust grains in size ranges $0.001 < a_{\text{gr}} < 0.3 \mu\text{m}$ (e.g. Mathis 1990). The goal of this paper is to compare the properties of the interstellar dust grains inferred from *in situ* data with grain properties derived from observations of interstellar matter (ISM) in front of nearby stars, in order to understand the properties of interstellar dust grains in nearby interstellar gas and in the cloud surrounding the Solar System. Comparisons with presolar grains in meteorites, and interplanetary dust grains, highlight similarities and differences compared to interstellar grains. These combined perspectives provide an interdisciplinary glimpse of the dust grains embedded in the interstellar cloud flowing through the Solar System, or the “Local Interstellar Wind” as it has been nicknamed. In this paper, we will denote the interstellar cloud surrounding the Solar System as the “Local Interstellar Cloud” (LIC). The downstream (or, equivalently, downwind) directions are given in Appendix A.

An interdisciplinary approach for understanding interstellar dust grains is employed, based on comparing *in situ* spacecraft data (§3) and astronomical data (§5) to evaluate the gas-to-dust mass ratio in the LIC. The criteria for separating interstellar dust grains from interplanetary dust grains observed by the Ulysses and Galileo satellites are reviewed (§3.1). The impact events selected from the combined Galileo and Ulysses interstellar dust datasets

(§3.2.1) provide a data set from which the mass distribution of the *in situ* detected events can be determined and compared with the predictions of standard astronomical models (§3.2.2). Such a comparison is original to this paper. These events then provide a basis for estimating the gas-to-dust mass ratio for detected grains (§3.3). Alternative methods of obtaining information on interstellar dust grains in the Solar System are discussed, including possible thermal infrared emission features and excess carbon from pickup ion observations (§3.4). Gas-dynamic models are used to evaluate the exclusion of small interstellar grains at the heliopause and by interactions with the solar wind within the heliosphere (§4), as a function of the adopted heliosphere model (§4.1) and grain charge and gyroradii (§4.2, 4.3). In Section 4.4 it is shown that grain destruction processes are unlikely to be significant in the time it takes for grains to traverse the region between a heliospheric bow-shock and the heliopause. The dynamics of interstellar dust grains within the heliosphere, including the counter-effects of radiation pressure and gravitational focusing, are discussed in Section 4.5. Section 5 investigates the properties of interstellar dust grains in interstellar material near the Sun, including grain properties derived from mass “missing” from the gas phase (§5.1) when absorption line data are compared with the nominal reference abundance for the material. Astronomical observations of ϵ CMa and λ Sco, combined with an assumed reference abundance for the gas, give a range for the values of the gas-to-dust ratio in the LISM which constrain either the reference abundances or the gas-dust mixing history (§5.1). Enhanced abundances of refractories (§5.1) and inhomogeneous abundances in the LISM are present in the LISM (§5.1,5.3). These are consistent with the destruction of dust grains by interstellar shocks, and grain destruction models yield the shock velocity (§5.4). Presolar grains in meteorites may constitute only a small fraction of the interstellar particles, but are discussed in search of insights about the grain size and distribution and composition (§6). In Section 7 we discuss the implications of our comparison between *in situ* versus remotely detected interstellar dust grains in the LISM. We will conclude that

dust grains are overabundant in the cloud feeding interstellar grains into the Solar System, in comparison to the sight-line averaged LIC cloud component observed towards ϵ CMa. The higher column density diffuse clouds towards λ Sco (and 23 Ori) are consistent with the *in situ* results, however, indicating possible homogeneities. Consequently, we look at the dynamic separation of grains and gas (§7.3), and consider the possibility that a portion of the grain population has not exchanged material with the gas phase. Some consequences for dust grain evolution follow from the detected large mass tail on the interstellar dust grain mass distribution (§7.4), and grain models (§7.2). Finally, we discuss constraints placed on the reference abundance of interstellar gas by the comparisons between *in situ* and astronomical data (§5.1).

In several sections of the paper, for ease in reading, supporting material is given in appendices. Appendix A discusses LIC properties. More detail is given on the upstream direction that provided the basis for selecting the *in situ* events (Appendix B). Observations of the weak polarization of optical light towards nearby stars are the only direct data on nearby interstellar dust grains and are summarized (Appendix C). The interstellar absorption line data, drawn from the literature, which provide the basis for the understanding the LIC dust component discussed in §5 are presented in Appendices D.1 and D.2.

Unless otherwise indicated, interstellar dust grains are assumed to be spherical with density $\rho=2.5 \text{ g cm}^{-3}$. The conclusions in this paper, which focus on differences in the gas-to-dust mass ratios determined from *in situ* versus astronomical data, generally are not affected by this choice of the bulk grain density, which is somewhat uncertain. The main use of this bulk density is to provide an estimate of the grain-size range which corresponds to the measured grains, for a limited grain model. Exploring other grain models is beyond the scope of this paper.

2. Interstellar Cloud Surrounding the Solar System

The comparison of dust grains observed inside versus outside of the heliosphere requires an understanding of both the density of interstellar gas in the cloud surrounding the Solar System, and of the exclusion of charged interstellar grains from the heliosphere. Gas density is required to calculate the gas-to-dust mass ratio for the *in situ* grain population. Heliosphere models are constrained by solar wind ram pressure and by the density, ionization, temperature and magnetic field of the surrounding cloud. The interstellar magnetic field strength governs the exclusion of the smallest particles from the heliosphere. The physical properties of the diffuse warm low density cloud surrounding the Solar System are summarized in Table 1; the basis for the selection of these values is discussed in Appendix A. A number of primary importance to the results of this paper is the total space density of the cloud feeding dust grains into the heliosphere, as this is the number to which the *in situ* data are normalized. Based on a range of data and models, this number is unlikely to be more than 50% larger than the adopted value, and the uncertainty does not alter the conclusions of this paper.

The cloud surrounding the Solar System is a fragment of a cloud complex sweeping past the Sun from the direction of the center of Loop I (Frisch 1995). Within about 35 pc of the Sun, column densities do not exceed $\sim 10^{19} \text{ cm}^{-2}$, and are an order of magnitude larger in the galactic center hemisphere than the anti-center hemisphere. The material within about 35 pc of the Sun is referred to as local interstellar matter (LISM).

3. Interstellar Dust Properties from Spacecraft *In Situ* Observations

Grün et al. (1994) have shown that the direction of motion of interstellar dust grains is consistent with the direction of motion of interstellar He^o also measured with Ulysses (Witte

Table 1: Properties of Interstellar Cloud Surrounding Solar System

Item	Adopted Values	Notes
$n(\text{He}^o)$	0.015 cm^{-3}	1
$N(\text{H}^o)/N(\text{He}^o)$	14.7	2, 3, 4
$n(\text{H}^o+\text{H}^+)/n(\text{He}^o+\text{He}^+)$	10	10
$n(\text{H}^o)$	0.22 cm^{-3}	Inferred, 15
$n(\text{H}^+)$	0.10 cm^{-3}	5, 6, 7, 12, 15
Downstream direction in solar rest frame		
Ecliptic coordinates	$\lambda=74.7^\circ \pm 1.3^\circ$, $\beta=-4.6^\circ \pm 0.7^\circ$	1
	$V=24.6 \pm 1.1 \text{ km s}^{-1}$	
Upstream directions:		
Solar rest frame, galactic coordinates	$l=2.7^\circ$, $b=+15.6^\circ$	
	$V=-24.6 \pm 1.1 \text{ km s}^{-1}$	
LSR rest frame, galactic coordinates:	$l=315^\circ$, $b=-3^\circ$	14
	$V=-19.4 \text{ km s}^{-1}$	
Temperature	6,900 K	11
Magnetic Field	1.5–6 μG	9, 13, Appendix A

Notes: 1. Witte et al. 1996, and Witte (private communication). 2. Dupuis et al. 1995. 3. Frisch 1995. 4. Vallerga 1996. 5. Slavin and Frisch 1998. 6. Gry and Dupin 1996. 7. Wood and Linsky 1997. 8. Section 1. 9. Frisch 1990 (estimated value). 10. Savage and Sembach 1996b. 11. Flynn et al. 1998. 12. Lallement and Ferlet 1997. 13. Linde (private communication). 14. This value is based on subtraction of the “standard” solar motion of 19.5 km s^{-1} towards the direction $l=56^\circ$, $b=+23^\circ$ from the observed LISW heliocentric velocity vector. If the “best” solar motion of 16.5 km s^{-1} towards $l=53^\circ$, $b=+25^\circ$ had been subtracted instead, the LSR inflow direction of the local interstellar wind would be $V=-18.2 \text{ km s}^{-1}$ from $l=324^\circ$, $b=-1^\circ$ (e. g. Frisch 1995). 15. Puyoo and Jaffel 1998

et al. 1993). Appendix B provides the criteria by which interstellar dust grains are selected from the Ulysses/Galileo data sets. With a larger data sample, we will show (Appendix B) that this result holds when a quantitative χ^2 -fit of the data is performed. Grün et al. (1994) determined the mean number-flux of interstellar grains through the heliosphere as $1.5 \cdot 10^{-8} \text{cm}^{-2} \text{s}^{-1}$, and that the most abundant grains in these data have masses of $3 \cdot 10^{-13} \text{g}$, corresponding to grain radius $a_{\text{gr}} \sim 0.3 \mu\text{m}$ for density 2.5g cm^{-3} and spherical grains. We will compare the observed grain mass distribution with the standard MRN model mass distribution for interstellar dust, and show that in the detected population of grains with $a_{\text{gr}} > 0.3 \mu\text{m}$ contribute most of the mass. The exclusion of smaller grains by heliospheric interactions is discussed in Section 4.3.

3.1. Criteria for Identifying Interstellar Dust Grains

One of the prime objectives of the Ulysses dust detector was to search for interstellar dust, which must be distinguished from interplanetary dust particles (Grün et al. 1992a). The main distinction between these two dust populations was thought to be their respective spatial distributions: interplanetary dust is strongly concentrated to the ecliptic plane while the interstellar dust flux should show little dependence on ecliptic latitude. However, it was fortuitous that interstellar dust was even more easily identified. Delays in the launch date of Ulysses lead to an out-of-ecliptic orbit that was perpendicular to the flow of interstellar dust. Thereby, the spin of the spacecraft gives rise to the maximum modulation of the interstellar impact rate as a function of spin angle and allows an accurate determination of flow direction. In addition the aphelion of the Ulysses orbit was on the side of the Sun where interstellar flow was opposite to the orbital motion of interplanetary dust. Thus, the interplanetary dust flux which displays a strong radial gradient was at minimum and the interstellar flux was the dominant flux. For a launch date three years earlier as

originally planned, little interstellar dust would have entered the detector because then the descending node of Ulysses' orbit would be directed parallel to the upstream direction. In such a configuration the dust detector points would always point nearly perpendicular to the interstellar direction.

Micron-sized interstellar dust particles passing through the solar system have been positively identified and separated from interplanetary dust by meeting three criteria (Grün et al. 1994, Baguhl et al. 1996):

1. After the Jupiter flyby Ulysses observed a dominant flux of dust particles arriving on prograde orbits from the opposite direction of interplanetary dust. The detected impact direction is compatible with grains from outside the Solar System, if we assume that these grains enter the Solar System from close to the upstream direction of the interstellar wind (Witte et al. 1993). The determination of the upstream direction of interstellar dust is discussed in Appendix B (see also Baguhl et al. 1995).
2. Despite a big uncertainty in the impact speed determination (factor 2, Grün et al. 1992b) by the Ulysses dust detector, most particles had speeds in excess of the heliospheric escape speed. To detect high impact velocities we use the total impact charge measured by the detector. The total charge produced by an impact is highly sensitive to the impact velocity (Grün et al. 1992b). High impact charges can also be produced by slow interplanetary grains with large masses. The flux of these grains is low beyond 3 AU, so we can neglect them when considering data that were collected at the 5 AU heliocentric distance of Jupiter.
3. As discussed above, the flux of these interstellar particles was independent of ecliptic latitude (Baguhl et al. 1996) in contrast to interplanetary dust that is strongly concentrated towards the ecliptic plane and the inner solar system. Dust emanating from the Jovian system is localized to the Jovian vicinity (Grün et al. 1993).

Consideration of these factors demonstrates that these *in situ* particles are not interplanetary dust particles. What about other more exotic Solar System dust populations, like dust from the Kuiper belt or the Oort cloud?

The Kuiper belt, thought to be the source of the short period comets, is located outside the orbit of Neptune (Flynn 1994, Jewitt and Juu 1993, Jewitt and Luu 1995). It is considered to be the remnant of the outer parts of the protoplanetary disk, and consequently the Kuiper belt objects are concentrated near the ecliptic plane and move in nearly circular orbits with typical radii of 40 – 80 AU. Thus, most of the dust produced in the Kuiper belt, if it should reach the inner heliosphere at all, would come from directions near the ecliptic plane and from all heliospheric longitudes, which is not compatible with the dust observations at medium and high solar latitude. The same argument can be used to exclude other potential Solar System sources located inside the heliosphere.

Another population that could mimic the kinematic parameters of interstellar dust are grains originating in the Oort cloud of comets. A very straightforward argument negates any likelihood of the Oort cloud as a significant source of dust particles in the inner heliosphere. The Oort cloud occupies a spherical shell at an average solar distance of $R_{\text{Oort}} \approx 5 \cdot 10^4$ AU. With an estimated total mass (M_{Oort}) of 20–40 Earth masses (cf. Weissman 1996) it is considered to be the source of the long-period comets. Mutual collisions and perhaps other mechanisms operating in this cloud are producing small grains that could become accommodated in the interstellar gas flow and reach the inner heliosphere from the same direction as the gas. However, the contamination of grains from the Oort cloud in the interstellar grain flux must be very small, as the following argument shows. If the total mass flux of interstellar dust of $f_{m,\text{IS}} = 2 \cdot 10^{-20}$ g cm⁻² s⁻¹ (see section 3.3) should all come from the Oort cloud, its life-time would be given by

$$t_{\text{Oort}} = \frac{M_{\text{Oort}}}{4\pi R_{\text{Oort}}^2 f_{m,\text{IS}}}. \quad (1)$$

The result is $t_{\text{Oort}} < 10^5$ years, showing that the Oort cloud would survive only a very short time if a significant fraction of the observed interstellar flux were produced by it.

3.2. Characteristics of Interstellar Dust in the Heliosphere

3.2.1. *The Galileo and Ulysses Interstellar Dust Datasets*

Using the criteria for interstellar impacts given in section 3.1, we define the subsets of the Galileo and Ulysses data which make up the interstellar dust datasets. For this, we use Ulysses data after Jupiter flyby until March 1996, excluding the ecliptic crossing, and Galileo data on its way to Jupiter between 3.5 AU and the arrival in the Jovian system. The dataset was collected either in-ecliptic outside 3.5 AU or at higher heliocentric latitudes. In both the Galileo and Ulysses data, impacts caused by Jupiter stream particles have been identified and removed Grün et al. (1993;1996b).

The dataset from which the interstellar dust grain mass distribution will be derived (§3.2.2) was selected by grain impact direction. The criterion is: All impacts that were not identified as Jupiter stream particles (Grün et al. 1993), and that are compatible with coming from within $\pm 70^\circ$ of the upstream direction of the interstellar wind (ignoring possible deflections by heliospheric interaction) plus a 10° -margin for uncertainties in the upstream direction, are candidates for interstellar impacts. Since Ulysses returned to the inner Solar System, β -meteoroids and interplanetary grains have to be removed from the data collected by Ulysses in this phase of its mission within a few AU of the Sun. Possible impacts from β -meteoroids originating above the poles were removed by restricting the impact charge to be larger than $1 \cdot 10^{-13}$ C. In the Ulysses dataset, impacts by interplanetary grains on orbits with small inclinations (as reported by Grün et al. 1997) are removed by cutting out the data that were collected $\pm 60^\circ$ around the ecliptic crossing, because in this

phase of the mission Ulysses was on the Sun side where interstellar dust and interplanetary dust grains came from the same direction. The remaining set of detected impacts defines our interstellar dataset for the determination of the mass distribution. This dataset contains 337 events detected by Galileo. We note that for 28 of them, the impact direction was not detected. Ulysses contributes 313 particles, 8 of them without direction information. For the determination of the upstream direction we have to choose the impact velocity criteria so as not to introduce a directional bias. The impact velocity criterion for the Ulysses dataset from which the upstream direction is derived is that the event, is not identified as a Jupiter stream event and that the impact charge has to be larger than $1 \cdot 10^{-13}$ C. This means that if the impacting particle had a mass of 10^{-13} g, the impact velocity has to be larger than 20 km s^{-1} . In order to have a constant relationship between measured rotation angle and upstream direction we chose the period of time between Jupiter flyby in February 1992 and May 1993 where the geometry didn't change significantly. During this phase Ulysses was outside 3 AU.

3.2.2. Mass Distribution

Figures 1 (a) and (b) show the number of interstellar grains per logarithmic mass interval detected by Galileo and Ulysses.

We determine the mass of the grain that caused the detected event by using an impact speed of 26 km s^{-1} and calculate the mass from the impact charge amplitude using the calibration given in Gruñi et al. (1995). The detection mass threshold for grains with impact velocities of more than 20 km s^{-1} is 10^{-15} g. The mean masses are calculated as sample means, i.e. the total mass of the detected grain sample divided by the number of events, they are: $\bar{m} = 2 \cdot 10^{-12}$ g for Galileo and $\bar{m} = 1 \cdot 10^{-12}$ g for Ulysses data (for $a_{\text{gr}} \sim 0.5\text{--}0.6 \text{ }\mu\text{m}$ for $\rho = 2.5 \text{ g cm}^{-3}$ and spherical grains). The mean masses are larger

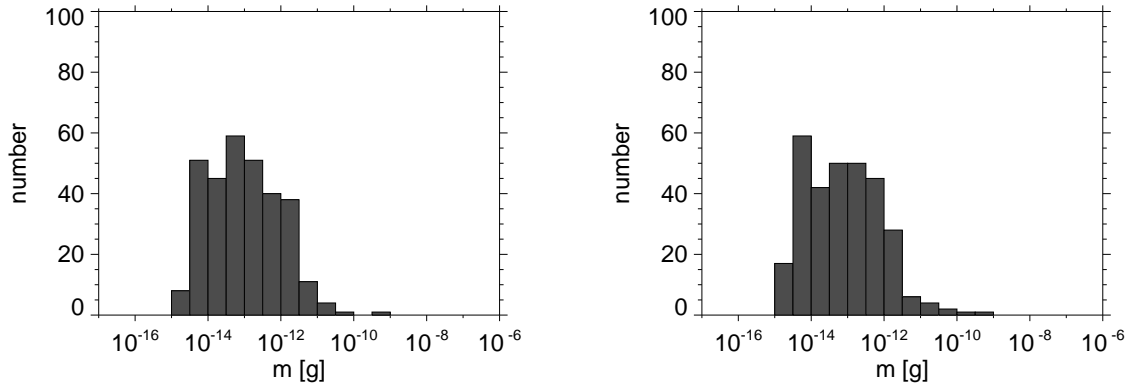


Fig. 1.— Mass histograms of interstellar grains detected by (a) *Galileo* with 309 impacts, and (b) *Ulysses* with 305 impacts. These histograms plot the number of interstellar grains per logarithmic mass interval. The drop in count rates at masses below 10^{-15} g (corresponding to grain radius $0.07 \mu\text{m}$ for spherical grains with density 2.5 g cm^{-3}) results from a decrease in instrument sensitivity for 20 km s^{-1} grains.

than the typical masses reported by Grün et al (1994). ($m_{\text{typ}} = 3 \cdot 10^{-13}$ g), because the heavy grains dominate the total mass. The two histograms do not differ significantly, so we combine both datasets to calculate the mass-density distribution. Small particles (one or two orders of magnitude above the detection threshold) are under-abundant compared to a MRN distribution (see below) even if we do not introduce a minimum mass for the identification of interstellar particles (c.f. Grün et al. 1994). This is the result of filtration of small grains by the solar wind magnetic field (§4.5) and in the heliopause region (§4.3). As expected, the number of particles drops steeply for large masses (Figure 1).

The observed grain population is compared with the expected interstellar dust grain population, using the empirically derived MRN size distribution (Mathis et al. 1977) as a strawman example. For comparison, the size distribution of Kim, Martin and Hendry (Kim et al. 1994) looks like the MRN distribution for smaller grain sizes, turns over at radii of

$\sim 0.2 \mu\text{m}$, and falls steeply out to $1 \mu\text{m}$ radius. The MRN size distribution is given by

$$\frac{dn}{da_{\text{gr}}} = n_{\text{H}} \mathcal{N} a_{\text{gr}}^{-\alpha}, \quad (2)$$

with $\alpha = 3.5$, \mathcal{N} is a normalization constant, n_{H} the number-density of hydrogen atoms, and the grain radius a_{gr} ranges from 5 nm to 250 nm. We use $n_{\text{H}} = 0.3 \text{ cm}^{-3}$ (cf. §3.3) and \mathcal{N} is chosen to fix the MRN gas-to-dust mass ratio to 100. To compare the *in situ* distribution with the MRN distribution we consider the differential distribution of mass-density per logarithmic mass interval $n_m(m)$. For grains with a MRN size distribution this mass distribution (mass-density per logarithmic mass interval) is given by

$$n_{\text{MRN}}(m) = \frac{mdn}{d(\log m)} = \frac{\ln 10 \mathcal{N} n_{\text{H}}}{3} \left(\frac{3}{4\pi\rho_{\text{gr}}} \right)^{\frac{1-\alpha}{3}} m^{\frac{4-\alpha}{3}}. \quad (3)$$

We assume spherical grains with bulk density $\rho_{\text{gr}} = 2.5 \text{ g cm}^{-3}$.

From equation (3) follows that for $\alpha = 4$ the mass-density per logarithmic mass interval is constant.

The mass distribution of all *in situ* detections shown in Figure 2 does not indicate any steep cutoff for particles with masses larger than $1.6 \cdot 10^{-13} \text{ g}$ (or $a_{\text{gr}} = 0.25 \mu\text{m}$ for spherical grains with $\rho_{\text{gr}} = 2.5 \text{ g cm}^{-3}$) as postulated by the MRN distribution. There is limited overlap of the MRN and the *in situ* distributions in the interval $10^{-15} \text{ g} \leq m_{\text{gr}} \leq 1.6 \cdot 10^{-13} \text{ g}$, but in general the number of observed grains in this interval is much lower than predicted by the MRN distribution. For $m_{\text{gr}} \geq 1.6 \cdot 10^{-13} \text{ g}$ the *in situ* distribution seems to extrapolate a MRN like power-law to grains with larger masses. For masses larger than 10^{-12} g the *in situ* distribution flattens and shows no further increase. At the low-mass end of the distribution in Figure 2, the events shown are above the sensitivity cutoff of $\sim 10^{-15} \text{ g}$. Since the total mass-density is given by the integral over the distribution function in Figure 2, it is clear that the large particles measured *in situ* dominate the total mass, as if also the case for an MRN size distribution of particles. The anomalies at both the small and large

ends of the observed grain population, when compared to predicted sizes based on starlight reddening measurements, leads us to examine later the screening of small charged grains by heliospheric plasmas (§4) and the decoupling of large grains from interstellar grains (§5.4, §7.3).

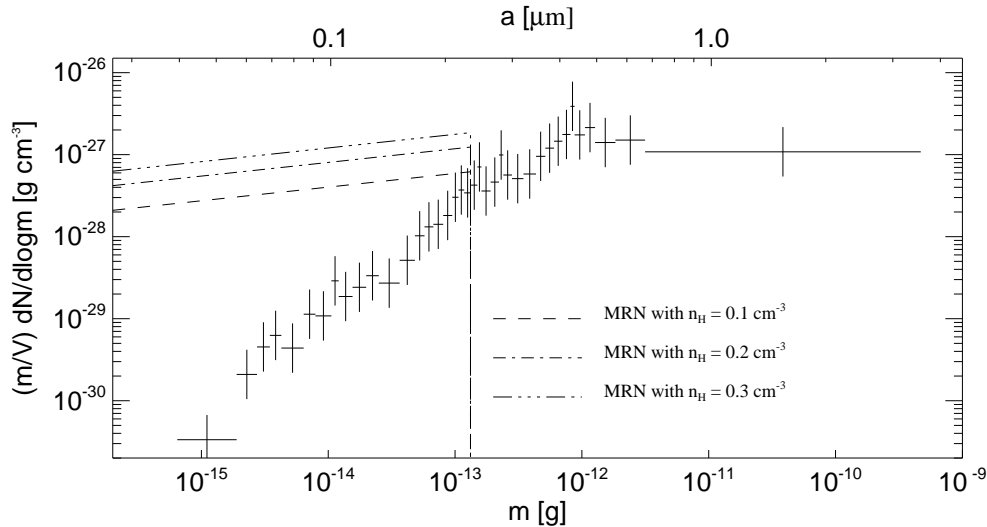


Fig. 2.— *Mass-density distribution per logarithmic mass interval of in situ particles. The dashed lines show the MRN distribution for three normalizations of the total mass density in the LIC, assuming a gas-to-dust mass ratio of 100. The vertical line gives the upper limit cutoff of the MRN distribution at $0.25 \mu\text{m}$, for spherical grains and assumed density 2.5 g cm^{-2} . The crosses give the value of the distribution function with error-bars which indicates the uncertainty of mass determination. Each data-point represents a collection of 16 impact events. The top axis gives the grain radius corresponding to the mass shown on the bottom axis, for spherical grains.*

3.3. LIC Gas-to-Dust Mass Ratio Implied by *In Situ* Measurements

In this section we derive the gas-to-dust mass ratio implied by the *in situ* detections. We also estimate the total mass of dust particles with masses greater than the mass of the

heaviest observed grains in the Ulysses and Galileo datasets, $\sim 10^{-9}$ g, making a guess about the mass distribution at the large end. The exclusion of small grains from the heliosphere by Lorentz force interactions with the solar wind and in the heliopause region is discussed (§4).

First we calculate the total mass-density $N_{m,\text{UG}}$ of interstellar grains measured by Ulysses and Galileo by integrating the mass distribution function shown in Figure 2. It follows that $N_{m,\text{UG}} = (7.5 \pm 0.8) \cdot 10^{-27}$ g cm $^{-3}$, which translates to a gas-to-dust mass ratio $R_{\text{g/d}} = (n_{\text{H}}m_{\text{H}} + n_{\text{He}}m_{\text{He}})/N_{m,\text{UG}}$ of $R_{\text{g/d}} = (94_{-38}^{+46})$ assuming $n_{\text{H}} = (0.3 \pm 0.1)$ cm $^{-3}$, where n_{H} and n_{He} are the number densities (cm $^{-3}$) of H and He respectively, m_{H} , m_{He} are the respective masses of H and He, and $n_{\text{H}}/n_{\text{He}}=0.1$. Note that this determination of the gas-to-dust ratio is independent of any assumptions about the reference abundance of the interstellar gas except that $n_{\text{H}}/n_{\text{He}}=10$, but it does assume that all helium is in the gas-phase. If we assume a relative velocity of the interstellar dust of 26 km s $^{-1}$ (e. g. Witte et al. 1996), we get a dust mass flux of $(2.0 \pm 0.2) \cdot 10^{-20}$ g cm $^{-2}$ s $^{-1}$. The $R_{\text{g/d}} = 94$ value compares favorably with generic gas-to-dust ratios in the interstellar medium (e.g. Spitzer 1978).

The extrapolation of the total mass-flux of interstellar grains observed within the Solar System to the densities in the interstellar cloud feeding this material into the Solar System leads to a lower limit, because if we assume that grains with masses smaller than $3 \cdot 10^{-14}$ g are missing from the *in situ* data because of Lorentz force filtration in the heliosheath and heliosphere (see section 3.2.3), the mass of these small grains must be added back to obtain the total mass of dust in the interstellar medium. Furthermore we note that focusing or defocusing effects by interaction with the solar wind magnetic field as described in section 4.5 do not affect the large ($a_{\text{gr}} > 1 \mu\text{m}$) grains which dominate the total mass-density. We also do not need to take into account gravitational focusing, because during the phases

when the Galileo and Ulysses data were collected, both spacecraft were far away from the region in which gravitational focusing can occur.

We now evaluate the total mass in the large end of the mass distribution. To do so, we correct for the mass of the excluded grains, with the hypothesis that the excluded grains obey a MRN mass distribution. We assume that the real mass distribution of dust grains in the LIC follows the MRN law for grains with $m_{\text{gr}} \leq 1.6 \cdot 10^{-13}$ g, and for heavier grains that the mass distribution function approaches a constant level of $1.5 \cdot 10^{-27}$ g cm⁻³ per logarithmic mass interval. The total mass-density of grains in the LIC will be the sum of $5 \cdot 10^{-27}$ g cm⁻³ from the MRN-sized grains (a number which includes the mass of the excluded grains) and $1.5 \cdot 10^{-27}$ g cm⁻³ from every mass decade to which the mass distribution is extrapolated. For example if we extrapolate to the radar meteoroids discovered by Taylor et al. (1996) with $m \approx 10^{-6}$ g, the contribution of the large grains would be $1 \cdot 10^{-26}$ g cm⁻³, which is comparable to the mass-density of the particles detected *in situ*. The total cross section density of the extended size distribution increases only a few per cent over that of the MRN distribution ($1.8 \cdot 10^{-22}$ cm² cm⁻³). Therefore the extinction, emission or scattering characteristics of interstellar dust are not much changed by the existence of the big particles. The maximum entropy extinction fitting procedure of Kim and Martin (1996) for dense clouds seems to require the presence of particles as large as 10 μm .

In order to estimate the total missing mass due to heliosheath and heliospheric filtration of charged grains, we look at the difference between the MRN curve and observed mass distribution over the entire measured mass range. This is equivalent to calculating the area between the upper predicted MRN-line in Fig. 2 and the observed particles (crosses in Fig. 2) of the distribution of the *in situ* particles between masses of 10^{-15} g and $1.6 \cdot 10^{-13}$ g. The result is that 98% of the number of the assumed MRN particles (equivalent to

$4.9 \cdot 10^{-27} \text{ g cm}^{-3}$) are removed by interactions of grains with the solar wind magnetic field and heliosheath plasma. These numbers are sensitive to the assumed input initial mass distribution for dust grains in the LIC, which is poorly known theoretically.

The smaller particles that are excluded from entering the heliosphere at the transition region ($a_{\text{gr}} < 0.01 \text{ } \mu\text{m}$, see §4.3) also have masses smaller than the 10^{-15} g detection threshold of the Ulysses and Galileo dust detectors (Grün et al. 1992b).

3.4. Alternative Methods to get Information on Interstellar Dust in the Solar System

3.4.1. Thermal Emission

Since the grains detected by Ulysses and Galileo are heated by the Sun, in principle the infrared radiation they emit should be observable (e. g. Grogan et al. 1996). The emission depends on the grain temperature and composition. Assuming the emissivity is independent of wavelength, the equilibrium temperature would be $278/\sqrt{R_{\text{sun}}}$ where R_{sun} is the distance from the Sun in AU. Taking into account the optical properties of astronomical silicates as given by Draine and Lee (1984), the temperature is enhanced by up to 50% for grains in the mass range $10^{-15} \leq m \leq 10^{-9} \text{ g}$ as detected by the spaceprobes.

The emission spectra of graphite and silicate interstellar grains was calculated by integrating over the line of sight, taking into account the temperature variation with distance from the Sun and assuming a uniform spatial distribution. The spectrum of graphite grains is rather featureless, while the silicate spectrum shows prominent $10 \text{ } \mu\text{m}$ and $20 \text{ } \mu\text{m}$ features which come from the hot grains near the Sun. The emission of grains in the outer Solar System where the *in situ* measurements have been made, dominates the spectrum at about $100 \text{ } \mu\text{m}$.

The zodiacal light is 1000 times greater than the emission we predict here for interstellar dust heated by the Sun. There remain two observational methods to detect this emission, however. First, the thermal emission from zodiacal cloud particles can be significantly decreased by 2 orders of magnitude by observing from the outer Solar System regions at distances greater than 3 AU from the Sun. Several space telescopes proposed both to NASA and the ESA would observe from this vantage point, where the emission of interstellar dust heated by the Sun would no longer be negligible. The second method is to search for distinct signatures of the dust. If the interstellar particles are composed of silicate material, then they are predicted to have strong 10 and 20 micron emission bands. The 20 μm band is so wide and close to the peak of the continuum spectrum that it probably could not be distinguished, but the 10 μm feature is more promising. Interplanetary grains have a 10 μm silicate emission feature that is weaker than interstellar grains (Reach et al. 1996). However, interplanetary silicates may also contribute to these features, making the identification of emission from interstellar grains difficult. In addition to the spectral signature, there are possible spatial and temporal signatures due to the interaction of the solar wind and the particles (Grogan et al. 1996) and gravitational focusing.

3.4.2. Pickup Ion Source

An opportunity to study the composition of the interstellar grains in the Solar System is possibly provided by a phenomenon, that the grains evaporate close to the Sun and the atoms get picked up by the solar wind after they have been ionized. Geiss et al. (1996) and Gloeckler and Geiss (1998) reported the detection of singly ionized carbon and nitrogen pickup ions by the Ulysses/SWICS experiment coming from an inner source near the Sun. Gloeckler and Geiss (1998) noted that four processes could contribute to producing the ions of the inner source: (a) Evaporation from interstellar grains when they come near to the

Sun; (b) evaporation from interplanetary grains, i.e. debris from asteroids and comets; (c) dust released from small, undetected comets; (d) multiply-charged solar wind ions absorbed by grains and desorbed again to form singly charged ions. Since the strengths of the partial sources (b), (c) and (d) ought to decrease with increasing latitude, it is likely that source (a), evaporation from interstellar grains, contribute most of the ions at high latitude. Thus we may expect that a more complete study of the latitudinal dependency of the C^+ , N^+ , O^+ fluxes and velocity distributions by Ulysses will provide an unambiguous identification of the ion population that is produced by evaporation from interstellar grains in the inner heliosphere. This would provide a way to estimate the content of semi-volatile components in these grains.

4. Interaction of Interstellar Dust Grains with the Heliosphere

In order to compare the gas-to-dust mass ratio values, $R_{g/d}$, as determined inside the Solar System (§3.3) against the values found for the LISM (§5.1), we must first understand the transversal of these grains across the heliopause region, and after that through the solar wind. Previous treatments of this topic include, e.g., Levy and Jokipii (1976), Wallis (1987) and Kimura and Mann (1998). Comparisons between interstellar dust grains observed within the heliosphere with the incident interstellar population provides a unique opportunity to tie together the properties of the interface between the solar wind dominated heliosphere and the surrounding interstellar cloud, the cloud itself, and the interstellar radiation field generated by stars in the LISM and beyond. The charging of the grains due to processes in the LIC determines how effectively the grains couple to the magnetic field as the field is swept into the heliospheric bow shock, compressed and then swept around the nose of the heliosphere. The structure of the field in the region between the heliopause and the bowshock and, in particular, the field strength, determine how grains with a given

charge-to-mass ratio will propagate. The far ultraviolet (FUV) radiation field, in particular that part of the field above 8 eV, plays a critical role in determining the equilibrium charge of the grains (as detailed below).

Grains which succeed in crossing the heliopause encounter the solar wind, where they are subject to Lorentz-force interactions as well as gravity and radiation pressure. Thus, the *in situ* observed dust grain size distribution will depend on the initial grain size distribution in the LIC, on the dynamics of grains injected into the heliosphere bow shock and heliosheath, and on grain charging rates inside and outside of the heliosphere. The interstellar magnetic field, FUV radiation field intensity, and solar cycle dependent solar wind properties all contribute to the ability of interstellar dust grains to penetrate the heliosphere, so that comparisons between *in situ* data and predicted incident grain mass distributions should provide important constraints on all properties.

4.1. Heliosphere Model

Dust grain traversal of the heliopause region must be determined using a heliosphere model, which includes both neutral ISM and an interstellar magnetic field. The self-consistent inclusion of neutral interstellar hydrogen into models describing the interaction of the solar wind with the LIC changes the structure of the heliosphere when compared to heliosphere models based on purely gas dynamical or MHD assumptions. Specifically, the neutral hydrogen mediated heliosphere is typically of much smaller extent than a non-mediated heliosphere because neutral gas is more compressible than plasma. This can be seen when the gas-kinetic models of Baranov et al. (1998) are compared with gas-dynamic models. To date, several models have been advanced which describe the two-dimensional (2D, Baranov and Malama 1993, Pauls et al. 1995, Zank et al. 1996) and three-dimensional (3D) Pauls and Zank (1997a) structure of the heliosphere while

retaining the dynamical influence of the interstellar neutral H component. Pauls and Zank (1997b) have developed a “convected field” model based on their 3D hydrodynamic models. Linde et al. have developed an MHD gas-dynamic model (Linde et al. 1997). We use a barely subsonic multi-fluid model for the heliosphere-ISM iteration. We use the Pauls and Zank (1997a,b) and Zank et al. 1996 models of the global heliosphere to make (i) a simple estimate of the grain sizes that will be excluded from the heliosphere, and (ii) use the observed lower limit on *in situ* grain size (§3.2.2) to estimate bounds for the LISM magnetic field strength. By balancing the length scale of the heliospheric boundary layer, in this case the separation distance between the bow shock and heliopause, with the Larmor radius of the dust grains, we can determine which dust grain sizes are likely to be swept around the heliosphere by the diverted LISM plasma component flow. Particles with gyroradii in excess of the boundary layer thickness will enter the heliosphere relatively easily owing to their weaker coupling to the interstellar plasma on these length scales. This comparison yields an estimate of the sizes of the excluded grains. It will be seen that these results do not change significantly when we use an MHD model which incorporates a weak interstellar magnetic field.

By assuming a LISM proton temperature $T = 7500$ K, a (supersonic) plasma inflow velocity of 26 km s^{-1} , and proton number density of 0.1 cm^{-3} , together with a neutral H interstellar density of 0.14 cm^{-3} , the 3D simulation of Pauls and Zank (1997a) yields a two-shock heliosphere, i.e., one in which a bow shock decelerates the impinging LISM flow and a solar wind termination shock, both of which are separated by the heliopause. While the temperature used in this model deviates from the best value (Table 1), these results are insensitive to that difference. The distance to the termination shock is ~ 95 AU at the nose and the distance to the bow shock is ~ 235 AU and the separation distance between the bow shock and termination shock is ~ 140 au. These figures can vary a little depending on parameters, and a typical separation length between the bow shock and the heliopause for

the various two-dimensional (2D) simulations is ~ 150 au. The inclusion of an interstellar and interplanetary magnetic field (Washimi and Tanaka 1996, Pauls and Zank 1997b, Linde et al. 1997) leads to a substantial increase in the strength of the magnetic field from the LISM to the heliopause. The weak perpendicular bow shock (compression ratio $r \sim 2$) approximately doubles the downstream magnetic field strength. In the heliosphere model used here, the LISM magnetic field increases nearly tenfold in an almost linear fashion to peak at the heliopause where it meets the interplanetary field. The interplanetary field is compressed at the termination shock, and also increases rapidly between the termination shock and the heliopause. For comparison, an MHD heliosphere model which directly incorporates an interstellar magnetic field and allows for field compressibility between the bow shock and heliopause gives an overall increase of the interstellar magnetic field between the heliopause and bow shock of about five for the assumed low density interstellar field ($1.5 \mu\text{G}$) (Linde et al. 1997). In this case, the relative distances of the termination shock, heliopause, and bow shock for the model adopted here are 120 au, 200 au, and 300 au. For a weakly magnetized ISM, the undisturbed interstellar field jumps weakly by about a factor of 2 at the bow shock, and rises to about $7.5 \mu\text{G}$ at the heliopause.

4.2. Grain Charge and Gyroradius

The dust charge may be expressed as

$$Q = eZ_{\text{gr}} = 4\pi\epsilon_0 a_{\text{gr}} U_{\text{eq}}, \quad (4)$$

where U_{eq} denotes the equilibrium grain surface potential, a_{gr} the radius of the (assumed) spherical grain, and the permittivity $\epsilon_0 = 8.859 \cdot 10^{-14} \text{ C V}^{-1} \text{ cm}^{-1}$. Thus the Larmor radius l_{gyr} of the grain depends on the grain radius quadratically,

$$l_{\text{gyr}} = \frac{m_{\text{gr}} v_{\text{d}}}{Q B} = \frac{\rho_{\text{gr}} a_{\text{gr}}^2 v_{\text{gr}}}{3\epsilon_0 U_{\text{eq}} B}. \quad (5)$$

In (5), B is the magnetic field, ρ_{gr} denotes the density of the dust grain and v_{d} is the grain velocity perpendicular to B . Guided by the results of detailed numerical calculations of the heliospheric boundary layer, we can express the variation of B between the bow shock and heliopause (to leading order along the nose) as, $B = Cx + rB_{\text{ISM}}$, where $0 \leq x \leq 150$ AU, B_{ISM} is the LISM magnetic field strength, $C \equiv (10 - r)B_{\text{ISM}}/150$ is a constant, and r is the compression ratio at the bow shock. This expression contains the result that B reaches $\sim 10B_{\text{ISM}}$ at the heliopause, but MHD calculations which include field compressibility indicate maximum compression factors of ~ 5 (Linde et al. 1997). A typical value for r , given our assumptions is $r \approx 2$. The grain density, ρ_{gr} , that we assume is 2.26 g cm^{-3} , appropriate for graphite grains. The speed of the Sun relative to the surrounding interstellar cloud, and thus the inflow speed of dust impinging on the heliosphere, is determined from observations to be $v_{\text{gr}} \simeq 26 \text{ km s}^{-1}$, and we assume $v_{\text{d}}=v_{\text{gr}}$ since the interstellar magnetic field direction is approximately perpendicular to the heliocentric flow vector. (The deflection of interstellar dust grains by magnetic fields in the heliosheath regions and heliosphere is discussed in detail by Landgraf, 1998.) We will return to a discussion of grain charge and gyroradius in Section 7.3 where the dynamic separation of interstellar dust and gas in the LISM is discussed.

The primary processes responsible for charging grains in the warm ($T \sim 10^4$ K) ISM are electrons and protons hitting and sticking to grains and photoelectric charging by photons from the FUV background. Ejection of secondary electrons due to electron and proton impacts are a minor effect at the temperature of the LISM, increasing the equilibrium potential (making it less negative) by $\sim 5\%$ in the absence of photoelectric charging. To determine U_{eq} we need to solve the equation for equal positive and negative grain charging rates as required by grain charge equilibrium, and relate those rates to the FUV flux and

the grain potential (Draine & Salpeter 1979). We may write this equation as:

$$g(\phi) = \sqrt{\frac{m_e}{m_p} \frac{s_p^{\text{eff}}}{s_e^{\text{eff}}}} g(-\phi) + \left(\frac{2\pi m_e}{kT} \right)^{1/2} \frac{1}{n_e} J_{\text{FUV}} \quad (6)$$

where

$$g(x) \equiv \begin{cases} e^x, & \text{if } x < 0 \\ (1+x), & \text{if } x \geq 0, \end{cases} \quad (7)$$

and ϕ is the grain potential parameter, $\phi \equiv \frac{eU}{kT}$; s_e^{eff} (s_p^{eff}) is the effective sticking coefficient for electrons (protons) including the reduction (increase) due to secondary electron emission; n_e is the electron number density in the LISM and J_{FUV} is the photoelectron current per unit grain area which depends on both the grain size and the FUV background flux averaged over the photoelectric yield. Ignoring the weak dependence of s_e^{eff} and s_p^{eff} on grain size, all of the dependence on the background FUV flux, the electron density and the grain size can be collected in the parameter ζ (McKee et al. 1987):

$$\zeta \equiv \frac{G_0}{n_e} \left(\frac{a_{\text{gr}}}{0.01 \mu\text{m} + a_{\text{gr}}} \right) \quad (8)$$

where G_0 is the yield-averaged FUV background normalized to Draine’s (1978) standard background. (As we discuss below, we now have reason to believe that G_0 is less than one). Thus by specifying ζ we can solve equation (6) numerically to determine ϕ and thus the charge on the grains, Z_{gr} .

We take the electron density in the Local Cloud to be 0.1 cm^{-3} (§2 and Table 1). With this choice, and a particular choice for G_0 , we can then determine U_{eq} . Expression (5) is then a relation between l_{gyr} and B_{ISM} . In Figure 3 we adopt a canonical LISM value for $B_{\text{ISM}} = 1.5 \mu\text{G}$ (Table 1), and plot the dust gyroradius as a function of a_{gr} across the heliospheric boundary layer. For a given value of G_0 (as noted in the figure), the range in gyroradius from bowshock (upper curve) to heliopause (lower curve) is shown in the figure. The increase in Larmor radius with increasing FUV flux is due to the decrease in the absolute value of the potential. As the FUV flux increases, the photoelectric current increases and the potential, which in most cases is negative, becomes more positive.

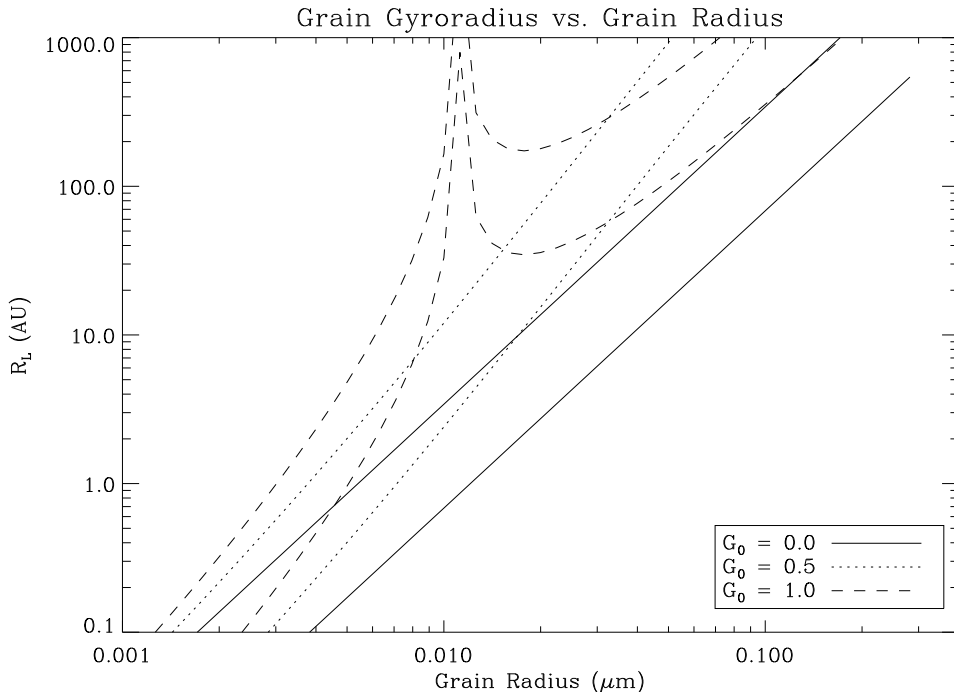


Fig. 3.— *Gyroradius vs. grain size for interstellar dust flowing into the heliosphere for an assumed ISM field of $1.5 \mu\text{G}$ and for different strengths of the FUV background parameter, G_0 . The upper curve for a given G_0 corresponds to the gyroradius at the bowshock and the lower curve is the gyroradius at the heliopause.*

The sharp upturn of the Larmor radius at $\sim 0.011 \mu\text{m}$ for the $G_0 = 1$ case is due to the crossing from negative charge for smaller grains to positive charge for larger grains. Note that further increases in the FUV flux ($G_0 > 1$) would continue to pull up l_{gyr} for small grains which were still negatively charged, but would pull down l_{gyr} for the large grains as their positive charge would increase. Formally, for large enough FUV flux ($G_0/n_e > \zeta_{\text{crit}}$) there is a grain size at which grains are neutral. Though it is unlikely that any significant number of inflowing grains will in reality be completely neutral, these results do point up the intriguing possibility that for a small range in grain size, the Larmor radii will be quite large. Thus it is possible that a particular size range of interstellar grains could be

significantly overabundant in the heliosphere. A detection of such a signature in the data would give us direct evidence on the charging of the dust, would tightly constrain the FUV flux in the Local Cloud and would allow much more reliable inferences for the large end of the dust size distribution.

4.3. Exclusion of Small Particles at the Heliopause

Figure 3 clearly demonstrates that grains smaller than $\sim 0.01 \mu\text{m}$ will be excluded from the heliosphere under most conditions. It is also evident that gyroradii of interstellar grains are strongly dependent on the strength of the FUV background. Taking $G_0 = 0.5$ as a reasonable value, we find that for grains of radius $a_{\text{gr}} = 0.04 \mu\text{m}$, the gyroradius is reduced from ~ 500 AU at the bow shock to ~ 100 AU at the heliopause. Thus, even for a relatively weak LISM magnetic field of $1.5 \mu\text{G}$, dust grains whose radius is less than $\sim 0.05 \mu\text{m}$ are likely to be excluded from the Solar System since they are sufficiently strongly coupled to the LISM plasma that they will tend to be diverted around the heliosphere. This exclusion limit is comparable to the lower limit of the mass sensitivity of the Ulysses and Galileo detectors (§3.2.2), and indicates that increasing the sensitivity of dust detectors on interstellar spacecraft will yield valuable science.

If one now turns expression (5) around by balancing l_{gyro} against the boundary layer scale length, one determines a relation between the interstellar magnetic field B_{ISM} and the grain radius, from which one can infer limits on the strength of the LISM magnetic field by observing which dust grains are excluded from the heliosphere. By adopting a separation length between the bow shock and heliopause of 150 AU (§4.1), we obtain Figure 4 in which B_{ISM} is plotted as a function of a_{gr} . The range of B_{ISM} values, which is a function of the variation of the magnetic field strength between the bowshock and heliosphere, is constrained by the pairs of lines for each value of G_0 as before. If dust grains of radius

$0.04\ \mu\text{m}$ are to be excluded from the heliosphere, then (again assuming $G_0 = 0.5$) the strength of the LISM magnetic field has to lie in the range $1\text{--}5\ \mu\text{G}$. The upper bound is in fact remarkably close to the estimated upper limit obtained by Gloeckler et al. (1997), from comparing pick-up ion data with heliosheath models. Arguments such as these can be used to derive the interstellar magnetic field from *in situ* detections of low mass interstellar grains in the heliosphere regions with future interstellar spacecraft.

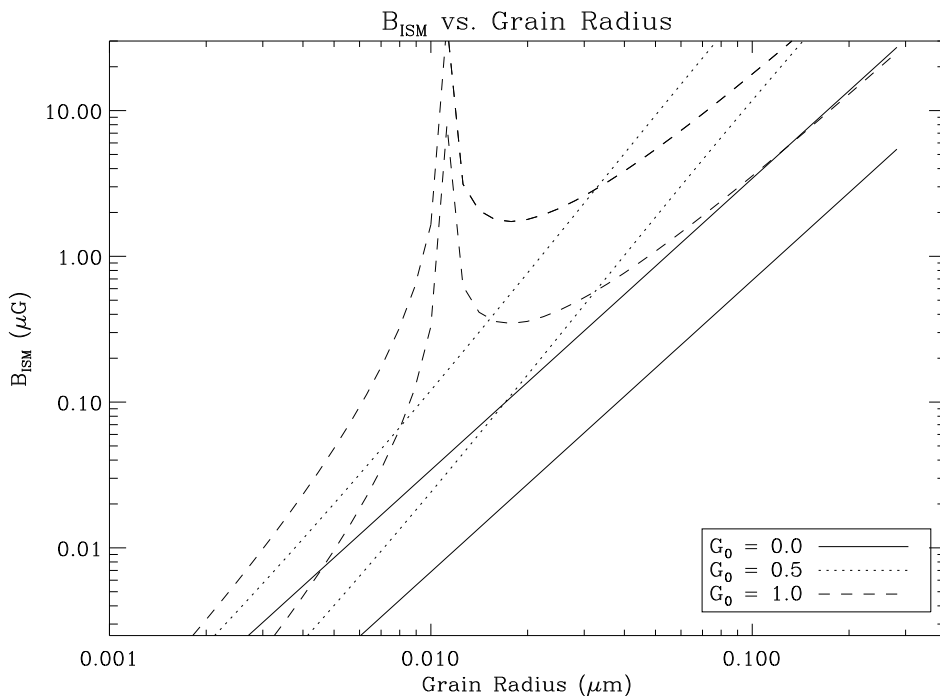


Fig. 4.— *Interstellar magnetic field vs. grain size for an assumed Larmor radius of 150 AU and for different strengths of the FUV background parameter, G_0 . We assume that grains with gyroradii less than 150 au, the approximate distance between the bowshock and the heliopause, will be excluded from the heliosphere. The upper curve for a given G_0 corresponds to the field if the grains are excluded at the bowshock and the lower curve is for exclusion at the heliopause.*

4.4. Heliosphere–ISM Transition Region and Dust Processing Timescales in LISM

The destructive processes that could operate on interstellar dust during its transport through the heliosheath regions and into the Solar System are thermal and inertial sputtering, and the grain-grain collisional processes of vaporization and shattering, similar to destruction processes in the LISM. these processes are insignificant at the low LIC densities, however. The threshold temperatures for the thermal sputtering of all likely grain materials are in excess of 100,000 K (Tielens et al. 1994), and thus will be unimportant at LISM temperatures of ~ 7000 K. Likewise, in the transition through the relatively weak bowshock and through the heliopause the temperatures ($T < 30,000$ K typically) are below the thermal sputtering threshold, and this process can therefore be ignored.

The threshold velocity for inertial sputtering, the process of grain erosion in gas-grain collisions, is of order 30 km s^{-1} . Thus, if the inflowing interstellar gas is rapidly slowed at the bowshock and the heliopause, and the larger momentum of the grains causes them to drift through this almost stationary gas, then inertial sputtering will be unimportant for the inflow velocity of 26 km s^{-1} . However, in these regions the dust will be betatron accelerated with respect to the gas, but the velocities (for LISM magnetic fields of order $5 \mu\text{G}$) will not result in significant inertial sputtering for the distances, densities and velocities appropriate to the transition from the LISM to the Solar System. For instance, in the more extreme environment of a 50 km s^{-1} interstellar shock wave in the warm ISM, with a density the same as that in the LISM, inertial sputtering results in the loss of only 0.1% of the grain mass, independent of grain radius (Jones et al. 1996). Again using the 50 km s^{-1} shock data (Jones et al. 1996) as an illustration it can also be shown that the effects of grain shattering in grain-grain collisions will be minimal in the bowshock and heliopause regions. Thus, other than filtering out the smaller grains, it is unlikely that there is significant

physical processing of the dust as it traverses the bowshock and heliopause regions.

4.5. Dynamics of Interstellar Dust Particles inside the Heliosphere

After the grains have penetrated the heliopause region, they enter the heliosphere in which they experience gravity, radiation pressure and the Lorentz-force caused by the solar wind magnetic field and their equilibrium charge in the heliosphere (surface-potential $U_{\text{eq}} = +5$ V) (Morfill et al. 1985). Due to the low density, the drag force by solar wind ions is negligible (Gustafson 1994). The relative strength of these forces depends in first approximation on the grain size, which determines the radiation pressure efficiency β (Gustafson 1994) and the charge-to-mass ratio Q/m_{gr} (Grün & Svestka 1996).

For large grains ($a_{\text{gr}} \geq 1 \mu\text{m}$), the Lorentz-force can be neglected. They are on hyperbolic Kepler-orbits. Gravitational focusing enhances their spatial density downstream of the Sun, whereas the density upstream of the Sun is very close to the value in the LIC. For grains with sizes of $\approx 0.4 \mu\text{m}$ radiation pressure dominates gravity and the grains get repelled by the Sun. Even smaller grains with $a_{\text{gr}} \approx 0.1 \mu\text{m}$ are dominated by the Lorentz-force (Levy and Jokipii 1976), which is in good approximation given by $\vec{F}_{\text{L}} = Qv_{\text{sw}}B_{\phi}\vec{e}_{\theta}$, where Q is the grain charge (Eq. 4), v_{sw} is the velocity of the solar wind particles, B_{ϕ} is the azimuthal component of the solar wind magnetic field and \vec{e}_{θ} is the normalized electric vector in polar direction. The large scale interplanetary magnetic field changes its polarity with the 22-year solar cycle. During one half of the solar cycle the Lorentz-force points towards the ecliptic north in the northern hemisphere and to the south in the southern hemisphere. Thus, the grains are defocused from the plane of the solar equator. In the second half of the solar cycle, the field-polarity is reversed and thus the particles in the northern hemisphere are deflected to the south and particles on the southern hemisphere are deflected to the north.

The solar cycle that started after the solar maximum around 1991 is defocusing until the next solar maximum in 2002. In both phases of the solar cycle very small grains experience a net deflecting Lorentz-force, because the magnetic field is at rest with respect to the frame of the solar wind. The size of the smallest grain which can penetrate to a given radial distance from the Sun depends on the solar cycle phase. The size-dependent filtering of interstellar grains within the heliosphere, which governs the size distribution of interstellar grains inside the heliosphere, depends on the total strength of the solar wind magnetic field and its perturbations at low latitudes and the equilibrium charge induced on the grains. In first approximation the filtration is independent of the solar wind velocity because the strength of the azimuthal component of the magnetic field decreases when the wind velocity increases leading to a constant Lorentz-force (Gustafson and Misconi 1979). The effect of filtration on the *in situ* mass distribution above the detection mass threshold (Figs. 1 (a), (b) and Fig. 2) is that submicron-sized grains are depleted with respect to bigger grains, explaining the relative absence of 10^{-15} to 10^{-13} g grains compared to the MRN distribution.

In an independent investigation of this problem, Kimura and Mann (1998) find similar results. They find that the influence of Lorentz forces on grains with masses less than 10^{-16} g (corresponding to $a_{\text{gr}} \sim 0.02 \mu\text{m}$ for density 2.5 g cm^{-3}) cause significant deflections of the grain propagation directions from the original flow.

5. Dust Grains in Local ISM

The diffuse ISM is an inhomogeneous environment (see, e.g., the review Dorschner and Henning 1995, or the array of diffuse clouds identified towards 23 Ori, Welty et al. 1999). In this section we tacitly assume a classical view of dust in the interstellar cloud surrounding the Solar System - i.e. that the dust grains of all sizes are formed by condensation from

interstellar gas of cosmic composition.

With this assumption we subsequently use observations of interstellar absorption lines in the spectra of nearby stars to determine the gas-to-dust mass ratio, $R_{g/d}$, for the cloud feeding interstellar dust grains into the Solar System. This derivation of $R_{g/d}$ requires two assumptions: first - that a nominal reference abundance describes abundances in the ISM and also that the total mass of the atoms “missing” from the gas phase is equal to the total mass of the interstellar dust grains. This standard method of determining the gas-to-dust mass ratio (e. g. Savage and Sembach 1996b; Meyer 1996) stands in contrast to values determined by modeling reddening and extinction curves, and scattered light (e.g., Spitzer 1978, Whittet 1992). For example, the widely-adopted Draine and Lee (1984) dust model which models extinction curves requires 300 ppm of carbon in graphite grains, and approximately solar abundances of Si, Mg and Fe. This results in a gas to dust ratio of ~ 110 with respect to H (or ~ 160 with respect to H+He). Large grains are not coupled to the gas (§7.3), and both very small and very large presolar grains from supernova and/or circumstellar envelopes of active giant stars are seen in meteorites (§6). If presolar type grains are mixed in with, or seed, the interstellar grain population, the basic assumption of this section is invalid. In other words, the dust mass can not be assumed to be equal to the mass of atoms “missing” from the gas phase, when the “missing mass” is calculated by comparing the total masses of the observed gas and hypothetical reference abundance gas.

The only direct evidence for interstellar dust grains in the cloud surrounding the Solar System is the optical polarization of light from nearby stars. These data are discussed in Appendix C. Because of the low total column densities, the polarization data do not directly constrain grain properties (e. g. Frisch 1991), but indicate silicate grains may be present (§5.2).

The abundances of refractory elements in the nearby ISM are enhanced with respect

to refractory abundances in cold interstellar gas (Frisch 1981). In Section 5.3 we show that these refractory depletions are relatively well behaved. Comparing LIC depletions with the range of Mg and Si depletions found by Fitzpatrick (1997), it is seen that the cloud around the solar system is a weakly depleted cloud, as confirmed by GD. An early model for the LIC proposed that the enhanced abundances of refractory elements, when compared to more distant cold clouds, are from the expansion of a shock front associated with the Loop I supernova remnant to the solar location (Frisch 1981, Frisch 1995). The destruction of LIC dust grains by a shock is modeled in Section 5.4.

5.1. Gas-to-Dust Mass Ratio in the LISM

Does the gas-to-dust ratio $R_{g/d}$ found from the *in situ* data agree with the value inferred from astronomical observations of the LISM? The gas-to-dust ratio in nearby interstellar gas is determined here for two sightlines through the LISM gas — LIC velocity component towards ϵ CMa and the warm neutral cloud complex towards λ Sco (which includes the LIC). These values are also compared to values for more distant diffuse gas seen towards 23 Ori. Total column densities towards ϵ CMa are an order of magnitude below values towards λ Sco (and 23 Ori), therefore in principle the LIC velocity component towards ϵ CMa (at -17 km s^{-1} , heliocentric velocity) should provide the best measure of abundances relevant to LIC dust grains. Together observations of gas-phase elements in these clouds constrain the dust grain mass and composition by comparison with a hypothetical total “reference” abundance of the element in the combined gas plus dust phases. We assume the difference between the mass of the gas with reference abundances and the mass of the observed gas is equal to the mass of the dust grains. This method of determining the gas-to-dust ratio in the LIC depends on the underlying assumption that both the reference abundance and gas-dust mixing are uniform in the ISM.

The gas-to-dust mass ratio is determined here using the relation:

$$R_{g/d} = \frac{\mathcal{M}_G}{\mathcal{M}_{R'} - \mathcal{M}_{G'}} = \frac{\sum_{i,gas} n_g(X_i)A_i}{\sum_{i,dust} n_d(X_i)A_i} = \frac{\sum_{i,gas} \text{PPM}_g(X_i)A_i}{\sum_{i,dust} \text{PPM}_d(X_i)A_i}. \quad (9)$$

The quantity \mathcal{M}_G is the total mass of all elements in the gas phase including He, and $\mathcal{M}_{G'}$ is the total mass in the gas phase of the elements excluding H and He. Note that He contributes $\sim 29\%$ of \mathcal{M}_G . The quantity $\mathcal{M}_{R'}$ is the total mass of all elements heavier than He in the hypothetical reference abundance gas. If all elements heavier than He were condensed onto the dust grains, the total mass of the dust grains would be $\mathcal{M}_{R'}$ (yielding gas-to-dust mass ratios of 64 and 101, respectively, for the solar and B-star abundances given in Table 5). Since H and He are not expected to be incorporated into the grains, the denominator is summed over elements heavier than He, while the numerator summation is over all elements (although heavier elements contribute relatively little mass to the gas). Here, only those elements are considered which have solar PPM abundances greater than 18, namely C, O, N, Si, Mg, Fe, and S. The quantity $n_g(X_i)$ is the space density in the gas phase of element X_i , $n_d(X_i)$ is the space density in the dust phase of element X_i , and A_i is the atomic mass of element i . The quantity $\text{PPM}(X_i) = \frac{N(X_i)}{N(\text{H})} 10^6$, with $\text{PPM}_g(X_i)$, $\text{PPM}_d(X_i)$ representing the number of atoms in “parts per million” in the gas and dust, respectively. The quantity $N(X_i)$ is the column density of element X_i . Uncertainties in the correct reference abundances to use for interstellar material are the major error in determining the gas-to-dust mass ratio in nearby ISM. Grain mass is dominated by a combination of the most abundant and heaviest elements.

The gas-to-dust mass ratio calculated for the LISM is highly sensitive to the assumed reference abundance pattern. Several recent studies find that the correct reference abundances for the ISM are $\sim 70\%$ of solar values (Snow and Witt 1995, 1996; Fitzpatrick 1996, Fitzpatrick 1997, Sofia et al. 1997, Meyer et al. 1997b, Cardelli and Meyer 1997). The strongest observation-based argument for using B-star reference abundances for the ISM

Table 2. Gas-to-Dust Mass Ratios, $R_{g/d}$

	<i>In situ</i>	ϵ CMa ¹	ϵ CMa ¹	λ Sco ²	λ Sco ²
Ref. Ab.	U/G ³	Solar	B-star	Solar	B-star
$\log N(\text{H}^\circ)$		17.30	17.51±0.07	19.23±0.05	19.23±0.05
$\log N(\text{H}^+)$		16.95 ⁴	17.15±0.20		
$\log N(\text{H}^\circ + \text{H}^+)$		17.46	17.66±0.21	19.23±0.05	19.23±0.05
$R_{g/d}$ ⁵	94 ⁺⁴⁶ ₋₃₈	427 ⁺⁷² ₋₂₀₇	551 ⁺⁶¹ ₋₂₅₁	137 ⁺¹⁶ ₋₄₀	406 ⁺⁵⁸ ₋₂₄₃

¹The column densities are from Dupin 1998 and Gry and Dupin 1996; the uncertainties are comparable to 2σ – 3σ (Gry, private communication).

²York 1983

³*In situ* values are determined from Ulysses and Galileo spacecraft data (§3.3).

⁴In this case, the ionized column density is estimated to be $\log N(\text{H}^+) = 16.95$ cm⁻², based on $n(e^-) = n(p^+) = 0.1$ cm⁻³ and $n(\text{H}^\circ) = 0.22$ cm⁻³. These values for $R_{g/d}$ are calculated using the column densities in Table 5.

⁵ $R_{g/d}$ is defined in eq. 9. The gas-to-dust mass ratio for λ Sco includes an estimate for Mg⁺ column densities based on the observed Fe⁺ column density and the correlation in Fig. 5. The uncertainties on $R_{g/d}$ are discussed in §5.1. For comparison, the diffuse WLW component towards 23 Ori (Welty et al. 1999 data, see §5.1) gives values $R_{g/d} = 127^{+13}_{-12}$ and 399^{+126}_{-120} for assumed solar and B-star abundances, respectively.

is based on observations of interstellar Kr, which has the dominant form Kr° in the ISM (the ionization potential is 13.99 eV), and which as a noble element should not be depleted onto dust grains (Cardelli and Meyer 1997). Cardelli and Meyer found that the interstellar Kr° abundance does not vary from sightline to sightline, and that it is independent of the fraction of hydrogen present in molecular form; they derived an interstellar Kr abundance in the solar vicinity of $\sim 60\%$ of the Solar System value. Observations of another undepleted element, N, in the form of N° , give N abundances $\sim 80\%$ solar. Uncertainties in the diffuse cloud ionization of N (with an ionization potential slightly above that of H), and in underlying oscillator strengths, however, render this result inconclusive (Meyer et al. 1997b). Observations of O° and C^+ , where both elements are grain constituents, suggest reference abundances $\sim 67\%$ and $\sim 60\%$ solar, respectively in interstellar gas (Meyer et al. 1997a, Sofia et al. 1997; Snow and Witt 1996). The gas-to-dust ratios in the LIC will be calculated for both assumed B-star and solar reference abundances.

The calculation of elemental abundances requires knowledge of H° column densities, which for the case of the LIC component towards ϵ CMa is somewhat uncertain because of strong stellar $L\alpha$ absorption lines. Despite these uncertainties, we will show in the following paragraphs that the high values for $R_{g/d}$ found for the LIC component towards ϵ CMa are typical of warm neutral clouds, suggesting that the H° column density uncertainties do not yield misleading conclusions. Three independent types of arguments indicate that the H° column density of the LIC component towards ϵ CMa has a value in the range $\log N(\text{H}^\circ)=17.3-17.5 \text{ cm}^{-2}$. Trace element measurements, including data on undepleted S, yield values $\log N(\text{H}^\circ)=17.30 \text{ cm}^{-2}$ if solar reference abundances are assumed, and $\log N(\text{H}^\circ)=17.51 \text{ cm}^{-2}$ if B-star reference abundances are assumed (Dupin 1998, Gry et al. 1995, Gry and Dupin 1996, Gry and Dupin 1998, collectively referred to as GD; Table 2). These low column densities are reinforced by observations of low column densities towards Sirius (α CMa), which is within $\sim 5^\circ$ of ϵ CMa but only 2.7 pc from the Sun. The Sirius

data give $\log N(\text{H}^\circ)=17.23_{-0.28}^{+0.17} \text{ cm}^{-2}$ for the LIC component (Bertin et al. 1995). The third support for low LIC column densities towards ϵ CMa are models of the ϵ CMa extreme ultraviolet spectrum, corrected for transmission through an interstellar cloud medium with solar abundances. These models require $\log N(\text{H}^\circ)<17.70 \text{ cm}^{-2}$ for the total H° column density (which is greater than the LIC cloud column density, Aufdenberg et al. 1998).

Values for $R_{\text{g/d}}$ for the LIC component in the star ϵ CMa and the LISM gas in λ Sco are given in Table 2. These values are based on equation 9, and the interstellar absorption line data presented in Appendix D.2 (which are based on data from Dupin 1998, Gry et al. 1995, Gry and Dupin 1996, Gry and Dupin 1998, York 1983). For ϵ CMa, $R_{\text{g/d}}=427_{-207}^{+72}$ and $551 \pm_{-251}^{+61}$ for assumed solar and B-star abundances, respectively. For λ Sco, $R_{\text{g/d}}=137_{-40}^{+16}$ and 406_{-243}^{+58} for assumed solar and B-star abundances, respectively. For comparison, for the diffuse interstellar “WLV” component found by Welty et al. (1999) towards 23 Ori, $R_{\text{g/d}}=127_{-12}^{+13}$ and 399_{-120}^{+126} for assumed solar and B-star abundances, respectively. The 23 Ori WLV component has ~ 0.3 dex more H° than λ Sco, and shows similar values for $R_{\text{g/d}}$.

The uncertainties quoted here are based on uncertainties in the input gas column densities. For the ϵ CMa data, the uncertainties represent the widest range of profile-fits yielding acceptable fits for the range of absorption lines under consideration (C. Gry, private communication). Although it is hard to translate the quality of results produced by profile fitting techniques (which require judgement calls) into root-mean-square deviations, the quoted accuracies should be good to at least the 2σ level, and possibly better. For the purposes of comparing the gas-to-dust mass ratios derived from astronomical data versus *in situ* data, we conclude that the resulting differences are real. This conclusion is also strongly supported by the high $R_{\text{g/d}}$ values found for the other diffuse cloud sightlines considered here. Note that small uncertainties on input gas-phase column densities translate into large fractional uncertainties in the dust PPM values for elements that are present

primarily in the gas-phase (see Appendix D.2).

From the high values of $R_{g/d}$ found in the preceding paragraph, for three separate diffuse clouds, when B-star abundances apply, we conclude that in this case there is a clear disagreement with the *in situ* value of 94. Clearly for B-star reference abundances, there is not enough mass “missing” from the gas phase to form the dust grain population observed by the spacecraft. Assuming, instead, solar reference abundances does not bring the gas-to-dust mass ratio for the LIC component towards ϵ CMa into agreement with the *in situ* data, but does bring $R_{g/d}$ in the higher column density material towards λ Sco and 23 Ori into agreement. Note that typical upper limits based on reddening curves in high column density sightlines give $R_{g/d} < 170$ (where the upper limit applies because large dust grains are not included in the calculation, Spitzer 1978).

The gas-to-dust ratio $R_{g/d}$ calculated from the missing gas mass is a fundamental tool that can be used to probe the properties of dust grains in the diffuse ISM. In the case of the LIC, the larger values of $R_{g/d}$ appear to be indicative of grain destruction by interstellar shock fronts, as is explored in Section 5.4. The somewhat higher column densities for the λ Sco and 23 Ori sightlines indicate that a blend of components is present, and that blend probably includes clouds with variable grain properties (e. g. Welty et al. 1995, Welty et al. 1996, Welty et al. 1999).

The ϵ CMa LIC component has no C available for the dust, a manifestation of the “carbon crisis” (e. g. Dwek 1997). Most of the dust mass is carried by refractories, with 45-50% of the dust mass carried by Fe, and 65-70% carried by Mg and Fe combined. The lack of carbon available for the interstellar dust grains, and the presence of SiC presolar grains in meteorites (§6.1), may indicate an additional carbon-rich grain source, beyond gas condensation from circumstellar dust grains.

5.2. Models of LISM Dust

In this section, we adopt a simple core-mantle grain model to explain the observed depletions. Following the approach given in Savage and Sembach (1996, SS), we use halo cloud sightline abundances to define the grain core, and assume that material in the grain beyond that required for the core composition must be contained in the grain mantle. Savage and Sembach use observations of halo stars to model the cores of interstellar dust grains. Subtraction of the core composition from the total dust composition given in Appendix D (Table 5) then yields the mantle composition. The LIC is among the least depleted sightlines and there is typically little mantle material on the grain cores.

For the grain core and solar abundances (based on SS halo star results), Mg : Si : Fe (and the ratio (Mg+Fe)/Si) are 1.1 : 0.6 : 1.0 (3.3). For B-star abundances, these ratios are 0.9 : 0.2 : 1.0 (8.6). For the little grain mantle material that remains on the dust in the ϵ CMa LIC component the solar reference abundances give Mg : Si : Fe are 0.5 : 0 : 1.0. Thus, it appears that the Si is to be found predominantly in the grain cores for the LIC. These ratios do not change significantly for B-star abundances. In contrast, the grain mantles in the cold cloud complex towards ζ Oph yield Mg : Si : Fe ((Mg+Fe)/Si) values of 1.4 : 2.6 : 1.0 (0.9) for abundances. For B-star abundances, these mantle ratios are 1.6 : 2.6 : 1.0 (1.0). These comparisons indicate that independent of the assumed reference abundance the LIC grains have been stripped of the silicate rich mantles found in cold cloud grains. Grain compositions are summarized in Table 3, using data from Appendix D.1.

In the cold cloud the mantle composition is enriched in Si (and Mg) when compared to the grain cores. However, grain mantles in the warm LIC cloud contain no Si and have very low mass in comparison to the cold cloud mantles, i.e., most of the original grain mantle material has been eroded into the gas phase. The enhanced abundances of refractories in the gas phase of the LISM (Frisch 1981, Vallergera et al. 1993) imply grain destruction

Table 3: PPM Abundances for Core-Mantle Dust Grains ^a

Element	Solar	Total Dust	Core ^b	Mantle	B-Star	Total Dust	Core ^b	Mantle
LIC								
Mg	38	28	27	1	25	18	12	6
Si	36	11	16	0	18.6	2.7	2.9	0
Fe	32	27	25	2	27	24	13	11
ζ Oph Cold Cloud^c								
Mg	38	37	27	10	25	23	12	11
Si	36	34	16	18	18.6	21	2.9	18
Fe	32	32	25	7	27	20	13	7

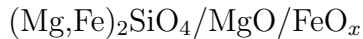
^a These data are based on the LIC component towards ϵ CMa (Table 5). The units are PPM, which represents the number of trace elements per 10^6 atoms. Solar reference abundances are from Savage and Sembach (1996), while B-star reference abundances are from Snow and Witt (1996), Meyer et al. (1997a, 1997b), and Sofia et al. (1997). ^b The core composition is given by halo star abundances in Table 7 of Savage and Sembach (1996). ^c From Savage and Sembach (1996).

in shock fronts, and the least refractory grain components in the mantle are eroded first. The material towards λ Sco represents a blend of components, and an intermediate case. Assuming solar reference abundances, Fe constitutes 46%, and 17% of the grain mass for the LIC cloud towards ϵ CMa and the LISM towards λ Sco, respectively. This indicates that there is relatively more silicate dust towards λ Sco than ϵ CMa, indicating less total grain destruction consistent with the models below. These data indicate that cores are Fe rich compared to the grain mantles.

Given the limiting chemical composition of silicates; i.e., a ratio $(\text{Mg}+\text{Fe})/\text{Si} \sim 1$ implies a pyroxene-type silicate composition, $(\text{Mg}+\text{Fe})/\text{Si} \sim 2$ implies a olivine-type silicate composition, $(\text{Mg}+\text{Fe})/\text{Si} > 1$ implies a mixed oxide/silicate composition. Using these criteria this implies that metal oxides, in association with some silicate material, are the components making up the dust grain cores. However, the fact that Fe and Mg are quite well correlated (§5.3) in the LISM indicates that the grain mantles, which have been eroded back into the gas phase, are silicates.

In order to satisfy the overall and sub-component structural and compositional stoichiometry of the dust phase one can invoke a ‘silicate’ grain core and mantle structure with mineralogical composition which, for the least refractory mantle component, is independent of the reference abundance adopted because one measures directly the composition from the gas phase abundances of the atoms eroded from the grains. However, the grain core composition is sensitive to the adopted reference abundance. The following schematically illustrates the likely dust phases and their approximate compositions:

Core – mixed Olivine-type silicate and oxide phases:



Mantle – Pyroxene-type silicate phase:



Studies indicate that the silicon in interstellar dust seems to be preferentially incorporated into a less refractory mantle phase, and that the metals Mg and Fe are generally in the more resilient core (e.g. Savage and Sembach 1996b, Tielens 1998). The good correlation between Mg and Fe column densities in the LISM reinforces this conclusion (next section). For the LIC cloud, the paucity of Si in dust mantles indicates that the dust mantle component has mostly been eroded into the gas. Thus, the differentiated ‘silicate’ grain structure, which is consistent with the observed depletions in cold clouds, will give rise to a differential rate of return of the elements to the gas through the effects of sputtering in supernova-generated shock waves. Silicate grains appear to be the main carrier of interstellar polarization, and therefore may explain the polarization of light of nearby stars (Appendix C). If solar reference abundances are correct, the relatively low values for $R_{\text{g/d}}$ towards λ Sco indicate a mixture of clouds where at least one cloud contains grains which have retained their silicate mantles, and therefore polarize starlight.

5.3. Variations in LISM Abundance Patterns

The differences in $R_{\text{g/d}}$ between LISM towards λ Sco and ϵ CMa and the likelihood that the LISM has been shocked (Frisch 1981, also see §5.4), suggest abundance variations may be present in the LISM gas, which is the nearest $\sim 10^{19} \text{ cm}^{-2}$ column density of gas. In warm gas, the refractory elements Fe and Mg are sensitive tracers of the site of grain destruction in shocks, and therefore should be spatially correlated. This follows from the fact that in cold clouds virtually all Fe and Mg are in grains, so that the destruction of a few percent of the grain mass changes gas phase abundances by large amounts. Also, if the main contribution to observed Fe and Mg in the gas phase comes from grain destruction, Fe and Mg should be well correlated in the LISM. Figure 5 shows this to be true, where points

plotted are drawn from the data in Appendix D.1, Table 6. In addition, the good correlation seen between Fe^+ and Mg^+ column densities indicates that column density uncertainties due to line saturation are relatively insignificant. Previous studies of depletions give similar results over longer sightlines (e.g., Fitzpatrick 1997, Fitzpatrick 1996).

In section 7.3 it is shown that frictional drag couples gas and dust poorly (scale sizes ~ 14 pc for $a=0.1 \mu\text{m}$ grains), so that when shock fronts both transport gas and destroy grains, local variations in the both gas-to-dust mass ratios and refractory abundances may result on sub-parsec scale-sizes.

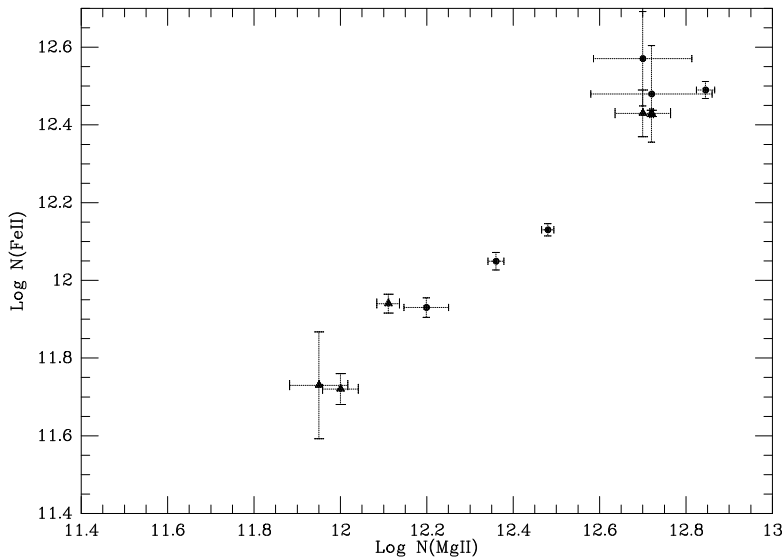


Fig. 5.— *Interstellar Fe^+ versus Mg^+ column densities are plotted for nearby stars. The data are from Table 6. Components plotted as circles or triangles indicate velocity components that are or are not (respectively) at the LIC cloud velocity (§5).*

In contrast, variable grain destruction in the LISM would be manifested by a poor correlation between Fe^+ (or Mg^+) and H° . Such a poor correlation is found in Fig. 6, based on data in Appendix D.1, but an alternative explanation invoking variable ionization would also explain this poor correlation.

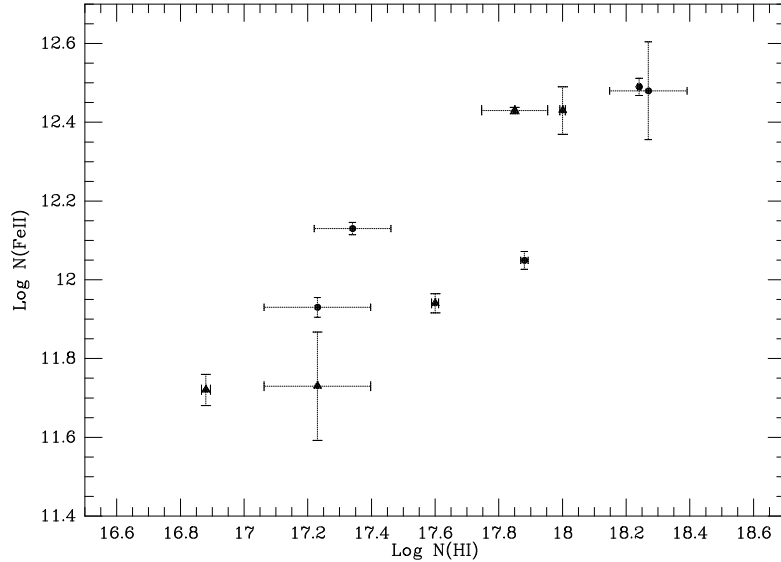


Fig. 6.— *Interstellar Fe⁺ versus H⁰ column densities are plotted for nearby stars. The data are from Table 6. Symbols same as Fig. 5.*

5.4. Shock Fronts, LIC Grain Survival and Size Distributions

Simple basic models for a shocked LISM have now been presented (Frisch and York 1991; Grzedzielski and Lallement 1996; Sonett et al. 1987), but these models do not include shock velocity-dependent grain destruction. Low velocity shocks ($\sim 20 \text{ km s}^{-1}$ with respect to preshock gas) are used to explain velocity gradients in nearby interstellar gas (Frisch and York 1991; Grzedzielski and Lallement 1996), and a high velocity shock model has been invoked to explain enhancements in the ^{10}Be isotopes deposited in ice cores ($V \sim 100 \text{ km s}^{-1}$, and a thickness of the order of 1 pc) (Sonett et al. 1987).

The enhanced abundances of refractories in interstellar gas are generally attributed to the destruction of interstellar dust grains by passing supernova-generated shock fronts. Using the shock models and results of Jones et al. (1994, 1996) we have calculated the depletions of the elements C, Si, Mg and Fe for unshocked dust, and for dust subjected

to shocks of velocity 50, 100, 150 and 200 km s⁻¹ the results are shown in Figure 7. The depletions in nearby interstellar gas can be used to constrain the likely velocity to which nearby interstellar material may have been shocked. Given the depletions found locally along the lines of sight toward ϵ CMa and λ Sco presented in Appendix D (Table 5, and also Table 2) the results in Figure 7 can be used to place constraints on the velocities of shocks which accelerated and processed the local dust grains. As indicated by the squares with error bars in Figure 7, the Si and Mg abundances toward ϵ CMa indicate that the LIC dust grains have been processed through a shock with a velocity $V \sim 110\text{--}220$ km s⁻¹. For this same line of sight the gas phase Fe abundances indicate a shock of velocity $V \sim 90\text{--}100$ km s⁻¹. The latter velocity may be a poor indicator because the results of Jones et al. (1996) are probably not valid for the shock processing of dense, Fe-rich grains which would undergo enhanced sputtering destruction (cf. the results for Fe grains in Jones et al. 1996). Indeed, if the data are to be believed then it appears that the Fe and Mg in interstellar dust may be more resistant to erosion by sputtering than Si. For the λ Sco line of sight the indicated shock velocities are much smaller and are of the order of $V \sim 0\text{--}70$ km s⁻¹. The origin for this discrepancy may result partly because the warm cloud complex towards λ Sco is a blend of several components (Welty et al. 1996), including both the weakly depleted LIC and pockets of more depleted gas.

6. Presolar and Interplanetary Dust Grains

Our knowledge of the elemental and isotopic composition, and grain history and sizes, for presolar dust grains found in primitive meteorites, and for interplanetary dust particles (IDPs), is far more precise than our understanding of the similar properties for interstellar dust grains. We briefly discuss these data sets in search of insights into the origin and properties of interstellar dust grains.

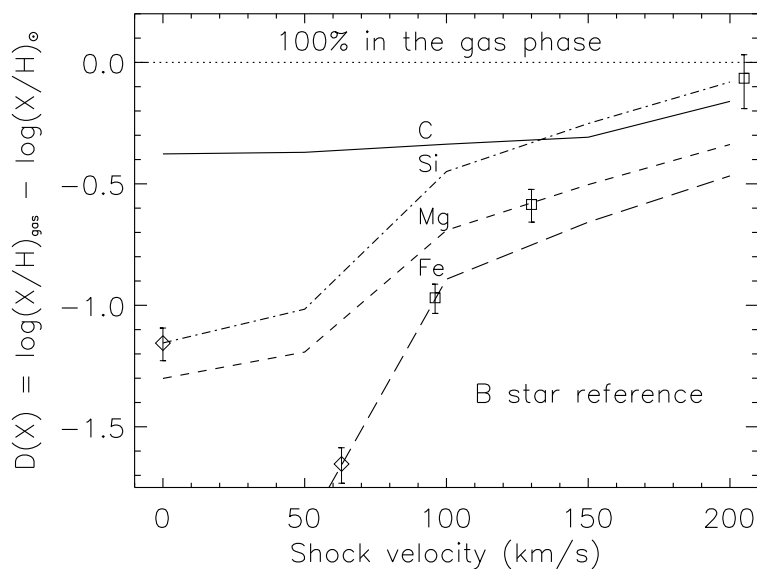


Fig. 7.— *Elemental depletions $\delta_{\text{H}}(X)$ for C (solid), Si (dash-dotted), Mg (short-dashed) and Fe (long-dashed) as a function of shock velocity for the B-star reference abundance core-mantle grain model of Section 5.2. The level of grain erosion was derived from the results of Jones, Tielens and Hollenbach (1996). Also shown ‘tied’ to the depletion curves at appropriate velocities are the depletions for the lines of sight toward ϵ CMa (squares with error bars) and λ Sco (diamonds with error bars), these data are taken from Table 2.*

6.1. Presolar Grains

While most of the material that went into the making of the Solar System was thoroughly processed and mixed, thus losing isotopic heterogeneity and all memory of its origin, small quantities of refractory dust grains survived the events that led to the formation of the solar system and such grains have been found in primitive meteorites (Anders and Zinner 1993; Zinner 1997; Ott 1993). They can be distinguished from other matter in the Solar System primarily on the basis of their anomalous isotopic compositions and they are believed to have formed in stellar outflows and in supernova ejecta. Presolar grains identified in primitive meteorites to date include diamonds, silicon carbide (SiC), graphite, silicon nitride (Si_3N_4), corundum (Al_2O_3), and spinel (MgAl_2O_4). Moreover, SiC and graphite grains carry small inclusions of Ti-, Mo-, and Zr-carbides (Bernatowicz et al. 1996). Although the presolar grains are older than 4.6 billion years they can provide useful insights into the properties of interstellar grains. Cosmic-ray exposure ages of presolar SiC grains have been estimated from the amount of cosmogenic ^{21}Ne produced from cosmic-ray spallation of Si. Ages of up to 130 (and possibly 2000) million years have been inferred (Lewis et al. 1994), but uncertainties remain.

6.2. Isotopic compositions and stellar sources

The physical and isotopic properties and likely stellar sources of the presolar grains from meteorites are summarized in Table 4. The diamonds are the most abundant but least understood presolar grains. One reason for this is their small average grain size of only 2 nm that does not permit the measurement of the isotopic compositions in single grains. The most striking isotopic signature of the diamonds is the presence of an anomalous Xe component, so-called Xe-HL (Huss and Lewis 1995). This component shows the signature of the p- and r-process of nucleosynthesis (photonuclear reactions and rapid n-capture,

respectively), pointing to Type II supernovae as possible stellar source of at least a small fraction of the diamonds (Clayton 1989). Most SiC grains (“Mainstream”, about 90% of total) (Hoppe et al. 1994) show imprints of the CNO cycle (cf. Fig. 8), some He burning, and the s-process (slow n-capture) and these grains are believed to have formed in the outflows of low-mass (1-3 M_{sun}) C-rich asymptotic giant branch (AGB) stars. The isotopic compositions of the rare SiC X grains (about 1% of total SiC) (Amari and Zinner 1996) and the isotopically related silicon nitride grains (Nittler et al. 1995) require matter from the interior of massive stars and Type II supernovae had been proposed as the most likely stellar sources of these grains. Laboratory data indicate that SiC (in contrast to most silicates) dissociates under bombardment by ionizing particle radiation, so that SiC may not survive as isolated grains in the ISM. Graphite is isotopically distinct from SiC (Fig. 8, Hoppe et al. 1995, Travaglio et al. 1999). Most graphite grains show the signature of He burning and these grains appear to have formed in the outflows of massive stars, namely, Wolf-Rayet stars and, more likely, Type II supernovae. In addition, minor contributions from C-rich AGB stars and novae are evident. The isotopic compositions of most corundum and spinel grains (Nittler et al. 1997, Choi et al. 1998) are well explained by models of red giant and AGB stars (e.g., Boothroyd et al. 1994) and the O-isotopic compositions agree quite well with those measured in the atmospheres of such stars (e.g., Harris and Lambert 1986).

6.3. Grain sizes

Except for the diamonds, all types of presolar grains have sizes in the submicrometer- to micrometer-range (Table 4). These sizes are considerably larger than typical sizes of 0.005–0.25 μm for grains in diffuse clouds, which provide the absorption and extinction of starlight in diffuse clouds. However, presolar grains may contribute to the large end

Table 4: Types of Presolar Grains in Primitive Meteorites.

Mineral	Abund. (ppm)	Size (μm)	Isotopic Signature	Stellar sources
Diamond	1400	0.002	Xe-HL	Type II supernovae
SiC Mainstream	14	0.1-20	enhancements ¹ in ^{13}C , ^{14}N , ^{22}Ne , heavy trace elements	C-rich AGB stars
Graphite	10	0.8-12	enhancements in ^{12}C , ^{18}O extinct ^{44}Ti	Type II supernovae, (Wolf-Rayet stars)
Corundum	0.3	0.3-5	enhancements in ^{17}O depletion in ^{18}O	Red giant, AGB stars
SiC X grains	0.1	0.5-10	enhancements in ^{12}C , ^{15}N , ^{28}Si extinct ^{26}Al , ^{44}Ti	Type II supernovae
Silicon nitride	0.002	~ 1	enhancements in ^{12}C , ^{15}N , ^{28}Si extinct ^{26}Al	Type II supernovae

¹ Enhancement values are given relative to the Solar System isotopic composition.

of the mass distribution determined from the *in situ* measurements (§8.3.2.2), and radar micrometeor data (Taylor et al. 1996). While the measured sizes of SiC and graphite grains are considered representative for the true distributions in the meteorites, the measured sizes of the corundum and silicon nitride grains are probably biased and shifted towards larger grain sizes (Nittler et al. 1997) and are thus not representative for the true distribution within the meteorites. The size distribution of SiC has been studied in most detail. Variations among SiC from different meteorites are evident, pointing to the operation of a size sorting mechanism in the solar nebula. SiC from the Murchison CM2 meteorite tend to be larger than SiC from other meteorites. About 20% of all Murchison SiC is in the $> 1 \mu\text{m}$ and only about 4% in the $< 0.3 \mu\text{m}$ fractions (Amari et al. 1994). SiC from the Indarch (EH4) meteorite is considered to be more representative for SiC in the protosolar nebula (Russell et al. 1997). Indarch SiC is finer grained and almost entirely composed of submicron grains with 60% of the grains in the $< 0.3 \mu\text{m}$ fraction and only 4% in the $> 1 \mu\text{m}$ fraction.

6.4. Presolar silicates and GEMS

Presolar silicates have not been found so far in primitive meteorites. This is an outstanding puzzle, since interstellar dust grains with silicate mantles are required in diffuse material, including nearby ISM, both by abundance arguments (§5.2), and by observations of polarization in nearby stars (Appendix C). Bradley (1994) has argued that the chemical anomalies found in GEMS (“glass with embedded metal and sulfides”) from interplanetary dust particles present a viable model for the structure and composition of interstellar silicate grains. In response to this hypothesis Martin (1995) presented a detailed analysis of the strengths and weaknesses in this hypothesis. In favour of GEMS being a good model for interstellar silicate grains are the following arguments: 1) the irradiated surfaces could

be caused by cosmic rays and shocks in the ISM, 2) Fe, Mg and Si show differentiation consistent with interstellar depletions, 3) they contain SPM inclusions that are required by interstellar polarization models, and 4) they are dirty enough silicates to explain the interstellar extinction and absorption. On the contrary they are not without problems, the most important of which are: 1) they contain sulphur, but sulphur is essentially undepleted in the ISM, and 2) meteoritic pre-solar grains show no evidence of interstellar radiation damage.

Nevertheless, the presolar nature of GEMS remains uncertain as long as no isotope data are available. Silicates are expected to be the dominant dust in circumstellar shells of red giant stars (Gehrz 1989). But these circumstellar dust grains may be smaller in size and have therefore remained undetected in the study of meteoritic matter or, alternatively, they may have been destroyed in the solar nebula or in the meteorite parent bodies. Analysis of cometary matter appears to be important for identifying presolar silicates because comets are believed to contain the most primitive Solar System matter and a large fraction of the silicate grains contained in comets may be of presolar origin. This emphasizes the importance of the STARDUST mission which will allow us to analyze cometary matter in the laboratory.

7. Discussion

In this section we discuss the implications of the variations in local gas-to-dust mass ratios found from the *in situ* observations versus several astronomical sightlines.

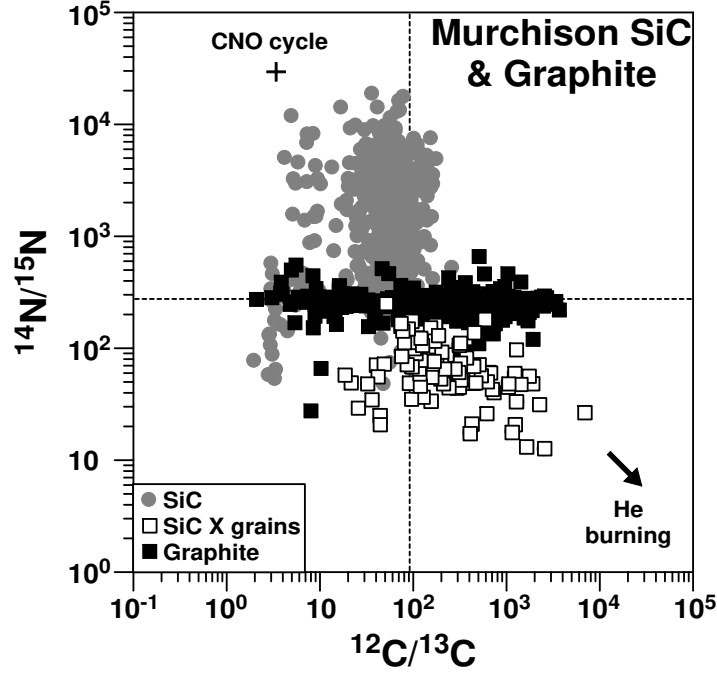


Fig. 8.— Carbon- and N-isotopic compositions of SiC and graphite grains from the Murchison meteorite. The dashed lines represent the Solar System isotopic compositions. Theoretical predictions for the CNO cycle and He burning are shown for comparison. The grain data are from Hoppe et al. 1994; Nittler et al. 1995; Hoppe et al. 1995; Hoppe et al. 1996.

7.1. LISM: $R_{g/d}$ and Reference Abundance

The *in situ* data give an upstream direction of interstellar grains which is close to the upstream direction of inflowing neutral LIC gas, indicating that the interstellar cloud surrounding the Solar System feeds these grains into the Solar System. The comparison of LISM absorption line data (§5.1) with *in situ* Ulysses and Galileo interstellar dust data leads to several conclusions about grain properties. The spacecraft observations show that dust is present in the LIC but with larger typical size ($a_{gr} \sim 0.5 \mu\text{m}$ for density 2.5 g cm^{-3} and spherical grains) than typical MRN grains. Since smaller grains are partially excluded

by interactions with heliospheric plasmas (§4), the $R_{g/d} \sim 94_{-38}^{+46}$ value determined from grains measured *in situ* will be an upper limit. This ratio depends on LIC properties, including total density ($n(\text{H}^0 + \text{H}^+) = 0.3 \text{ cm}^{-3}$, §2). Figure 2 shows that small grains expected in the MRN distribution ($m_{\text{gr}} \sim 10^{-15} \text{ gr}$, or $a_{\text{gr}} \sim 0.05 \mu\text{m}$ for spherical grains with density 2.5 g cm^{-3}), are in the range of the smallest masses of the grains detected by the *in situ* measurements, but the contribution of these small grains to the mass-density is low compared to what we would expect from the larger grains exhibiting an MRN distribution (Fig. 2). We partially interpret the deficit of small grains detected by the satellite observations, in comparison to the MRN mass distribution, to the interaction of these small grains with the solar wind magnetic field (grains with $a_d < 0.1 - 0.2 \mu\text{m}$, §4.5), and the interstellar magnetic field in the heliopause region (grains with $a_d < 0.05 \mu\text{m}$, §4.3). This indicates that although MRN particles must exist in the LIC, they can not be measured in the inner heliosphere where the Ulysses and Galileo measurements were made. So, to calculate the actual gas-to-dust mass ratio for the LIC, we have to add the contribution of the MRN particles, which were not detected *in situ*. If we estimate the gas-to-dust mass ratio of the LIC based on the *in situ* data, and add in the missing mass for the excluded MRN particles, then a value of $R_{g/d} = 56$ is found. The *in situ* detection is limited at large grain masses by the bad statistics, since large grains are rare by number. If we extend the mass distribution up to the mass of radar meteoroids (Taylor et al. 1996) the way we described it in Section 3.3, the gas-to-dust mass ratio will drop to 31.

In comparison, atoms missing from the gas phase in the LISM give gas-to-dust ratios of $R_{g/d} = 427_{-207}^{+72}$ for $\epsilon \text{ CMa}$, and $R_{g/d} = 137_{-40}^{+16}$ for $\lambda \text{ Sco}$, assuming solar reference abundances (§5.1). These two ratios are inconsistent with each other and both are larger than the value from *in situ* detections. The ratio is highly sensitive to the assumptions about the reference abundance, and the assumption of B-star abundances increases the gas-to-dust mass ratios determined from absorption lines data by factors 2–3, The uncertainties on

the $R_{g/d}$ values are large, due primarily to the relatively small fraction of the material contained in the grains (so that generally small fractional uncertainties in gas PPM values yield large fractional uncertainties in dust PPM values). However, the λ Sco and 23 Ori diffuse clouds, both with H° column densities typically ~ 19 dex or smaller, strongly support large values for $R_{g/d}$ for assumed B-star reference abundances. The $R_{g/d}$ values derived from the comparison of *in situ* and astronomical data yield somewhat better agreement for assumed solar, versus B-star reference abundances, but in the best data for the cloud feeding the grains into the Solar System, the data still is not adequate. We conclude that the assumption that all of the mass of LISM dust grains arises from the exchange of atoms with the gas phase may be incorrect. If B-star abundances are correct, we consider the possibility that part of the total mass contained in interstellar dust and measured *in situ* may not originate in the interstellar medium. In the second case, we could in principle turn the problem around and input known reference abundances to the ISM $R_{g/d}$ calculations, and compare the results with *in situ* data to give a direct determination of the relative proportions of the interstellar dust mass which may be attributed to direct stellar sources versus condensation in the interstellar medium.

7.2. Shocks and Grain Models

The LISM shows enhanced abundances of refractory elements in the gas phase (§5.3) when compared to more distant cold clouds, which is explained by the partial destruction of grains by shock fronts (§5.4). The destruction of grains by shocks explains the larger value in nearby interstellar gas of the gas-to-dust mass ratio, $R_{g/d}$, when compared to cold cloud values. For instance, the cold cloud complex towards ζ Oph has $R_{g/d}=103\pm_{-29}^{+13}$. It also explains the good correlation found between Fe and Mg column densities over several order of magnitudes of material (Figure 5). Even in the LIC over 80% of Fe and 58% of Mg

is locked into dust grains, causing small variations in dust mass to yield large variations in gas phase abundances.

When the composition of dust grains in the LIC towards ϵ CMa is compared to models for grain destruction in shock fronts, shock velocities on the order of $\sim 100\text{--}200$ km s $^{-1}$ are found. In the LISM gas towards λ Sco, with larger column densities, lower shock velocities are found. A general model presents grains consisting of a robust refractory core, coated with a mantle of more volatile material (e. g. Sofia et al. 1994, Savage and Sembach 1996a, Savage and Sembach 1996b, Jones et al. 1990, Li and Greenberg 1997). The composition of the robust core has been modeled using observations of selected clouds in halo star sightlines (Savage and Sembach 1996b), indicating that the robust grain core consists of mixed oxides and silicates, for either assumed solar or B-star abundances. If solar abundances are assumed, grain mantle material appears to be silicates; if B-star abundances are assumed then the core and mantle materials are not chemically distinct as would be consistent with grain destruction by interstellar shocks. This procedure is instructive, although recent discussions of interstellar grains as conglomerates of fluffy or multi-sized grains suggest alternate interpretations may be viable (e. g. Dwek 1997).

7.3. Dynamic Separation of Gas and Grains

The dust-to-gas ratios indicate the LIC may be inhomogeneous. There are several processes by which interstellar grains couple to the other components of the diffuse interstellar medium. The frictional scale l_{drag} over which the dust couples to the gas is given by the length it takes the grain to sweep-up its mass, m_{gr} , in form of interstellar gas (hydrogen, $m_{\text{H}} = 1.67 \cdot 10^{-24}$ g):

$$l_{\text{drag}} = \frac{m_{\text{gr}}}{A_{\text{gr}}(n_{\text{H}}m_{\text{H}} + n_{\text{He}}m_{\text{He}})}, \quad (10)$$

where A_{gr} is the cross-sectional area of the grain. This frictional length scale is proportional to the size, a_{gr} , of the grain and exceeds the extent of the local cloud (a few pc) already for most MRN-sized grains (e. g. $l_{\text{drag}} \sim 14$ pc for a grain with radius $a_{\text{gr}} = 0.1 \mu\text{m}$). This implies that the gas and dust in the local cloud are not in frictional equilibrium.

However, there is a much shorter length scale due to the coupling of the grains to the interstellar magnetic field. Interstellar grains in the local environment are electrically charged to about $U \approx 1$ V surface potential due to the dominant photo-electric effect from the background UV radiation field (§4.2). With grain charge and gyroradius given by Eqs. 4 and 5, a typical relative speed, v_{rel} of several km s^{-1} between the grains and magnetic field of strength $B \approx 1.5 \mu\text{G}$, the gyroradius l_{gyr} is less than the size of the local cloud even for micron-sized particles. Since the interstellar magnetic field couples closely to the ionized component of the interstellar medium, which in turn couples to the neutral component, interstellar grains are indirectly coupled to the gas. The effect is that gyrating dust particles have much increased path lengths in the local cloud and hence gas drag can thermalize the dust. However, if the relative speed between the magnetic field and the dust is much higher, as it would be in a supernova shock crossing, or the magnetic field is weaker, micron-sized grains would no longer couple to the magnetic field over dimensions of the local cloud. In these cases micron-sized and bigger particles would decouple from small grains and from the gas cloud. The different apex directions and much higher speeds of interstellar meteor particles (where 10^{-9} to 10^{-7} g, Taylor et al. 1996) support such a scenario.

Big particles (10^{-7} g, or $a_{\text{gr}} = 5 \mu\text{m}$ at density 2.5 g cm^{-3}) can travel several 100 pc before they are captured by the magnetic field and hence by the gas, i.e. big particles may be generated several 100 pc from the place where they are found. It is evident that big particles couple over much larger scales to the ambient diffuse interstellar medium (gas and fields) than do small particles, therefore, they may be compositionally unrelated to the gas

and the small particles, with independent origins. Consequently the actual dust to gas mass ratio may vary locally, and hence, the cosmic abundance (1% of the total mass in refractory dust) may be valid only over large scales (100 to 1000 pc). This conclusion qualifies the total gas-to-dust mass ratio derived here for the LISM but it does not qualify the relative comparison between the values derived from the *in situ* versus interstellar gas observations, since the grain size sampled *in situ* is dynamically bound to the gas being sampled by the interstellar absorption line data.

7.4. Effects of Big Particles on the Collisional Evolution of Interstellar Dust

The existence of large numbers of big particles (bigger than described by the MRN distribution) in the diffuse interstellar medium has profound consequences for evolution of interstellar material. Because of their relatively small geometric cross section they do not show up in optical observations. The total mass of dust grains not sampled by extinction measurements increases typically with grain radius, i. e. $m_{\text{gr}}/A_{\text{gr}}$, so large grain particles provide a significant reservoir for the production of smaller particles by collisions. This fact may help solve the mystery of the rapid destruction times of MRN-sized interstellar grains compared to the transport and injection times of grains into the diffuse interstellar medium.

Current models of dust processing in the ISM (Jones et al. 1996) indicate that grains with radii of order ten to a few thousand Angstroms (10^{-3} to $\sim 0.3 \mu\text{m}$) are rapidly fragmented into smaller particles due to the effects of shattering in grain-grain collisions in interstellar shock waves. This disruption occurs on timescales of order tens of millions of years. Thus, the presence of grains with sizes ranging from a few thousand Angstroms to those of order one micron in meteorites (§6), and in the detected interstellar dust in the Solar System, presents something of a challenge to current models of dust processing in interstellar shock waves. However, these same models (Jones et al. 1997) have also shown

that grains with radii much larger than one micron can survive fragmentation in shocks due to the underabundance of particles with radii large enough to cause their catastrophic disruption.

In this context, the dust destruction level of 2/3 for the LIC implies shock velocities greater than 200 km s^{-1} , and therefore the “large” MRN grains may actually fare better because the postshock compression is delayed and the large grain maximum velocities are reduced. In this case the thermal sputtering begins to destroy smaller grains. This may provide a partial solution to both the large average grain sizes observed *in situ* and the discrepant gas-to-dust mass ratios problems. If the LIC shock had velocity $>200 \text{ km s}^{-1}$, the shock would preferentially destroy small grains with respect to large grains by thermal sputtering. In this case, the $R_{g/d}$ value derived from *in situ* measurements may require little correction for the mass of the excluded grains, and therefore bringing the *in situ* determination closer to the values measured for the LISM with interstellar absorption lines. This issue is important since interstellar spacecraft will have to survive high-speed impacts with interstellar dust grains.

Two important parameters that determine the outcome of grain-grain collisions are the mass ratio, Γ , of the target and projectile grains and the relative velocity of the collision between the two. A catastrophic collision has been defined as a collision in which more than half of the larger (target) particle is shattered into smaller fragments (Jones et al. 1996). For the MRN dust size distribution (Equation 3) the mass range is about 10^5 . However, for the most disruptive collisions Γ ranges from 10^2 – 10^4 for $\sim 0.1 \mu\text{m}$ -sized target grains and $\sim 0.01 \mu\text{m}$ -sized projectile grains (Jones et al. 1996). Many (but not all) of the grain-grain collisions in a 100 km s^{-1} shock result in catastrophic shattering. The result is that a large fraction of the largest grains are completely disrupted in collisions with smaller particles. This leads to disruption timescales of about 5×10^7 years for $\sim 0.1 \mu\text{m}$ grains and

an accompanying steepening of the size distribution (Jones et al. 1996). The disruption timescale is short compared to the injection timescale of 2.5×10^9 years for the formation and ejection of stardust into the diffuse ISM (Jones and Tielens 1994). However, large grains can be re-formed in the dense regions of the ISM during cloud collapse and there is strong evidence for this grain growth in the denser ISM (e.g. Kim, Martin and Hendry 1994; Kim and Martin 1996).

In contrast, the particles observed by Galileo and Ulysses are as large or much larger than the typical interstellar dust particles required to explain the diffuse ISM extinction (e.g. Mathis 1990). It might be expected that they therefore have longer lifetimes in the ISM due to the underabundance of grains with radii sufficiently large to catastrophically destroy them in supernova-generated shock waves. However, this has yet to be demonstrated by detailed modeling. Hence one might consider that the large particles observed by Galileo and Ulysses could be considered as a conveyor belt that carries dust mass from their circumstellar sources to the diffuse ISM, where they become a reservoir for small particle formation by their fragmentation in grain-grain collisions in shock waves. Their ultimate demise would signal the end of the conveyor belt. Since big particles do not couple as closely to the gas as small grains (§7.3) they may form a background large grain dust distribution. Thus these interesting scenarios will have very important implications for the inhomogeneity of the ISM and the competition between large grain survival and dust re-cycling in the ISM. These complex processes would be worth investigating in greater detail.

8. Conclusions

In this paper we have produced five values, summarized in Table 2, for the gas-to-dust mass ratio for the local interstellar cloud. The first value is determined from *in situ*

observations of interstellar dust made by the Ulysses and Galileo spacecraft, and gives $R_{g/d}=94_{-38}^{+46}$ for the interstellar dust grains which are able to penetrate the heliosphere (typical grains with radii greater than $0.2 \mu\text{m}$). A set of values is determined for nearby interstellar gas based on interstellar absorption line measurements towards two stars, with the assumption that a standard reference abundance exists which describes the relative elemental abundances for the interstellar material, gas plus dust combined. This assumption is equivalent to assuming that all of the dust mass arises from the exchange of mass with interstellar gas. When the reference abundance is assumed to be that of B-stars, values for $R_{g/d}$ that are 4–5 times larger than the *in situ* value are found for the clouds considered towards ϵ CMa and λ Sco (Table 2). If the reference abundance is instead assumed to be solar, then the value for $R_{g/d}$ found towards λ Sco are comparable to the *in situ* value, considering uncertainties. However, the cloud best representative of the cloud surrounding the Solar System is the LIC cloud towards ϵ CMa, and $R_{g/d}=427_{-207}^{+72}$ found here is still a factor of three greater than the *in situ* value. Therefore, we conclude that although solar abundances yield the best match between astronomical and *in situ* determinations of $R_{g/d}$, regardless of the selected reference abundance it is likely that the interstellar dust grain population detected *in situ* contains grains which have not been formed exclusively by mass exchange with the LIC gas. This conclusion is entirely consistent with models of interstellar dust grains which invoke circumstellar and supernova sources for the interstellar dust grain population, although models of such sources are generally inadequate to explain observed grain abundances (e. g. Dwek 1998).

Both the *in situ* and extinction determinations of $R_{g/d}$ consider grains from all sources, whereas the $R_{g/d}$ calculated from “missing” interstellar gas does not include grain mass derived from stellar sources or any dust grain large enough to be inefficiently destroyed by shock fronts. Presolar grain data show us that stellar sources contribute over a large size range (§6), and therefore do not violate the *in situ* data. Based on these discussions,

some of the dust mass observed *in situ* must arise from an additional source which does not exchange mass with gas in the interstellar cloud surrounding the Solar System.

One possibility is that interstellar dust grains are seeded by refractory presolar-type grains from cool stars and supernova (§6). If this were true, then we could in principle turn the problem around and input known reference abundances to the $R_{g/d}$ calculations, and compare the results with *in situ* data to give a direct determination of the relative proportions of the interstellar dust mass which may be attributed to direct stellar sources versus condensation in the interstellar medium. However, the LIC gas has been shocked by high velocity shocks (§5.4) so that a pre-solar type grain population is also likely to have been shocked. Very little mantle material remains on the LIC dust grains because of destruction of these grains in shock fronts. A good correlation is found between Mg^+ and Fe^+ in nearby interstellar gas, suggesting that the mineral composition of the parent dust grains dominates the gas-phase abundances of these elements. In contrast, the poor correlation between Fe^+ and H° suggests either inhomogeneous ionization or poor dust-gas mixing on small spatial scales.

A second possibility is to look at the shock process itself. Large grains are inefficiently destroyed by shocks (§7.4). Therefore pockets of large grains may remain from the giant molecular clouds from which the subgroups of the Scorpius-Centaurus Association formed, with the grains captured in, and displaced towards the Sun, by the expanding superbubble shell surrounding this association (Frisch 1995). This process may contribute larger grains which have not exchanged mass recently with the LISM, since large grains are less likely to be thermalized in shock fronts (§7.4).

Once we are forced to invoke a distinct population of interstellar dust grains that does not interchange mass with interstellar gas, then we can not conclude that the better $R_{g/d}$ ratios found for the LISM data and assumed solar abundances indicate that solar

abundances are to be preferred over B-star abundances. On the other hand, if the λ Sco cloud complex were to be found to be relatively homogeneous, we would propose that the LISM cloud complex towards λ Sco, rather than the LIC seen towards ϵ CMa, is the cloud feeding dust into the Solar System. This is similar to saying that the Sun is immersed in the same interstellar cloud as α Cen, which does not appear to be the case.

Since we will conclude that the enhanced refractory abundances in the nearby interstellar gas indicate that the dust grains in the LIC have been shocked, it is of interest to search for correlations between the upwind direction of the LISW and external galactic kinetic phenomena. Frisch (1981) concluded that the Sun is located in the expanding superbubble shell from the Loop I supernova, based on the velocity of gas and enhanced refractory abundances in the LISM. When solar motion is removed from the LISW heliocentric flow vector, the local interstellar material is seen to flow from a direction corresponding to $l=315^\circ$ to 325° , $b=0^\circ$ to -3° (depending on the assumed solar motion; Frisch 1995; Table 1). This direction is close to the direction of the center of the Loop I 21 cm H $^\circ$ shell located near $l=320^\circ$, $b=+5^\circ$ (Heiles 1998). Based on the LIC dynamics and shock models (§5.4), the hypothesis that the Sun is embedded in a fragment of the expanding Loop I superbubble shell thus remains a viable hypothesis.

The results presented in this paper indicate that *in situ* measurements of the interstellar dust population in the heliosheath and interstellar medium would yield a high scientific return. When we have compared the gas-to-dust mass ratio found from the LIC cloud with the value expected from MRN grain populations only, we find 98% of the MRN-sized particles are missing from the population observed by Ulysses and Galileo, evidently because of exclusion from the heliosphere due to interactions with heliospheric plasmas. The MRN mass spectrum is selected as an example of an empirically derived interstellar dust grain distribution. These MRN-sized particles are the interstellar grain population most likely to

be exchanging mass with the interstellar medium. Measurements of the interstellar dust grain population outside of the heliosphere and in the heliosheath regions would capture the mass distribution of these interstellar particles excluded from the heliosphere. Comparisons of this distribution with the grain properties inferred from absorption line measurements of nearby stars would thus provide a valuable insight into the separate histories of large versus small interstellar dust grains, and into the sources of large interstellar dust grains which have not exchanged mass with the diffuse cloud surrounding the Solar System. If separate origins and history of large versus small interstellar grains are ascertained, and a grain population which does not exchange mass with the interstellar medium can be identified, this information would aid in understanding the chemical evolution of the Milky Way galaxy, external galaxies, and QSO absorption line systems.

The authors of this paper would like to thank the International Space Sciences Institute (ISSI) in Bern, Switzerland, for hosting workshops in January and October 1997 on the topic of “Interstellar Dust in the Solar System”. In particular, 15 of the co-authors would like to thank the 16th, Professor Johannes Geiss, for hosting this series of workshops. The results presented in this paper are based on the scientific discussions at these workshops. We would like to thank NASA grant NAG5-6625 for assisting US participants in travel support for the workshops. The authors gratefully acknowledge support for their research. GPZ was supported in part by a NASA grant NAG5-6469, JPL contract 959167 and a NASA Delaware Space Grant College award NGT5-40024. PCF has been supported by NASA grants NAG5-6405 and NAG5-6405. This research has made use of the Simbad database, operated at CDS, Strasbourg, France.

A. Adopted LIC Model

The properties of the interstellar cloud surrounding the Solar System are listed in Table 1. The basis for the choice of these values is given in this section. The physical properties of the cloud surrounding the Solar System can be derived from observations of interstellar matter within the Solar System (backscattered H^o and He^o radiations, direct detection of He^o, and the pickup ion and anomalous cosmic ray particle populations), from observations of ultraviolet and optical absorption lines in nearby stars, and from extreme ultraviolet observations of nearby white dwarf stars.

Ulysses observations of He^o within the Solar System give direct measurements of interstellar neutral He^o in the cloud surrounding the Solar System, since He^o is little affected by the traversal of the outer heliopause and heliosphere regions (e. g. Rucinski and Fahr 1989). The interstellar He^o density found from these observations is $n(\text{He}^{\circ})=0.016 \text{ cm}^{-3}$, and the downstream direction and relative Sun-cloud velocity were determined to be $\lambda=74.7^{\circ}\pm 1.3^{\circ}$, $\beta=-4.6^{\circ}\pm 0.7^{\circ}$ (ecliptic coordinates), and $V=24.6\pm 1.1 \text{ km s}^{-1}$ (Witte et al. 1996; Witte private communication). These values are confirmed by EUVE observations of the 584 Å backscattered glow (downwind direction $\lambda=76.0^{\circ}\pm 0.4^{\circ}$, $\beta=-5.4^{\circ}\pm 0.6^{\circ}$, $V=26.4\pm 1.5 \text{ km s}^{-1}$, Flynn et al. 1998). These values are converted into heliocentric and LSR velocities, in the galactic coordinate system, in Table 1. The upwind direction in the LSR ($l\sim 315^{\circ}$, $b\sim -3^{\circ}$) is close to the center of the Loop I 21 cm superbubble shell (at $l=320^{\circ}$, $b=+5^{\circ}$, Heiles 1998). Based on these dynamics, combined with the history of shocked grains in the LIC (Section 5.4), the conclusion that the Sun is embedded in a fragment of the expanding Loop I superbubble shell (Frisch 1981, 1995) remains a viable hypothesis.

Observations of nearby white dwarf stars in the extreme ultraviolet give a mean value

$$\left\langle \frac{N(\text{H}^{\circ})}{N(\text{He}^{\circ})} \right\rangle = 14.7 \quad (\text{A1})$$

where $N(X)$ is the column density (cm^{-2}) of element X (Frisch 1995, Dupuis et al. 1995, Vallergera 1996). For the stars with the two lowest foreground interstellar column densities, GD 71 and HZ 43, the ratios are 12.1 and 15.8, respectively. Combining these values, $n(\text{H}^{\circ})=0.19\text{--}0.25 \text{ cm}^{-3}$ is inferred for the H° spatial density in the LIC cloud, and we adopt the value $n(\text{H}^{\circ})=0.2 \text{ cm}^{-3}$. However, the LIC cloud is ionized, with the relative ionizations of H and He changing as a function of cloud depth. Hydrogen ionization increases towards the cloud edge with respect to helium ionization because of cloud optical depth effects. Therefore the ratio $N(\text{H}^{\circ})/N(\text{He}^{\circ})$ at the solar location should in principle be larger than the sightline averaged values if surrounding interstellar material is homogeneous, which in turn allows $n(\text{H}^{\circ})$ to be larger than this adopted value. Although inhomogeneities are clearly present (§5, 7), we do not consider the possibility that the inhomogeneities would yield higher neutral densities for the LIC. Radiative transfer models of the LIC give an electron (or proton) density of $n(e^{-})\sim 0.11 \text{ cm}^{-3}$ at the solar location (Slavin and Frisch 1997), a value in agreement with LIC values $n(e^{-})=0.09 \text{ cm}^{-3}$ (+0.23, -0.07) found towards ϵ CMa (Gry and Dupin 1995) and $n(e^{-})=0.11$ (+0.12, -0.06) cm^{-3} found towards α Aur (Wood and Linsky 1997), and $n(e^{-})=0.11 \text{ cm}^{-3}$ towards η UMa (Frisch 1998b). This gives values $n(\text{H}^{\circ})=0.21 \text{ cm}^{-3}$ and $n(e^{-})=0.11 \text{ cm}^{-3}$ for the LIC cloud, yielding a total LIC density of 0.32 cm^{-3} . The LIC temperature determined from recent observations of He° backscattered radiation in the Solar System is $6,900\pm 600 \text{ K}$ (Flynn et al. 1997), and this value is consistent with interstellar absorption line data in nearby stars (e. g. Lallement et al. 1995; Gry and Dupin 1996; Linsky et al. 1995). Observations of the neutral He flux by Ulysses give $T=6,100\pm 300 \text{ K}$ (Witte et al. 1996; Witte private communication).

The LIC magnetic field strength has not been directly determined. We adopt a magnetic field strength $B=1.5\text{--}2.0 \mu\text{G}$ because this value is consistent with the ordered component inferred from global pulsar data (Frisch 1990), comparisons between models and observations of hydrogen-wall $L\alpha$ absorption towards α Cen (Gayley et al. 1997), pick-up

ion data constraints (Gloeckler et al. 1997), and magnetohydrodynamic models of the heliosphere (Linde et al. 1997, §4.2).

Table 5. Elemental Abundances in Nearby Interstellar Gas

Element	Log N cm ⁻²	Denom. PPM ^{1,5}	< ----- Solar ² ----- >			< ----- B-star ----- >		
			Ref. Abun.	Gas PPM _g ^{1,10}	Dust PPM _d ^{1,6}	Ref. Abun.	Gas PPM _g ^{1,11}	Dust PPM _d ^{1,7}
ε CMa - LIC³								
C ⁺	14.20 ^{+0.05} _{-0.06}	H [°] +H ⁺	360	549±83	0	214	344±66	0
N [°]	13.20±0.01	H [°]	93	79±10	14±10	75	50±8	25±8
O [°]	14.15±0.03	H [°]	740	708±100	32 ⁺¹⁰⁰ ₋₃₂	457	442±73	15 ⁺⁷³ ₋₁₅
Mg ⁺	12.48±0.01	H [°] +H ⁺	38	10.5±1.0	28±1	25	6.5±1.0	18±1
Si ⁺ +Si ⁺⁺	12.87±0.03	H [°] +H ⁺	36	25 ⁺⁶ ₋₅	11 ⁺⁶ ₋₅	18.6	16±4	2.7 ^{+3.7} _{-2.7}
S ⁺	12.18–12.85	H [°] +H ⁺	19	5–25	0–14	12.3	3.3–15.5	0–9
Fe ⁺	12.13±0.02	H [°] +H ⁺	32	4.7±0.4	27±0.4	27	2.9±0.4	24.1±0.4
λ Sco⁸								
C ⁺	15.70 ^{+0.30} _{-0.70}	H [°]	360	295 ⁺²⁹⁶ ₋₂₃₉	65 ⁺²³⁹ ₋₆₅	214	295 ⁺²⁹⁶ ₋₂₃₉	0 ⁺¹⁵⁸ ₋₀
N ^{°11}	14.85±0.02	H [°]	93	42±5	51 ⁺⁵ ₋₆	75	42 ⁺⁶ ₋₅	33±5
O [°]	15.86 ^{+0.02} _{-0.01}	H [°]	740	427 ⁺⁵⁶ ₋₅₃	313 ⁺⁵³ ₋₅₆	457	427 ⁺⁵⁶ ₋₅₃	30 ⁺⁵³ ₋₃₀
Si ⁺	13.34±0.04	H [°]	36	1.3±0.2	34.7±0.2	18.6	1.3±0.2	17.3±0.2
S ⁺	14.28 ^{+0.06} _{-0.05}	H [°]	19	11±2	7.8 ^{+1.8} _{-2.2}	12.3	11±2	1.1 ^{+1.8} _{-1.1}
Fe ⁺	13.04±0.04	H [°]	32	0.6±0.1	31.4±0.1	27	0.6±0.1	26.4±0.1

Table 5—Continued

Element	Log N cm ⁻²	Denom. PPM ^{1,5}	< ----- Solar ² ----- >			< ----- B-star ----- >		
			Ref. Abun.	Gas PPM _g ^{1,10}	Dust PPM _d ^{1,6}	Ref. Abun.	Gas PPM _g ^{1,11}	Dust PPM _d ^{1,7}

¹PPM represents the number of atoms/ions per 10⁶ hydrogen atoms.

²The solar reference abundances are from Savage and Sembach (1996). B-star abundances are from Meyer et al. (1997a, 1997b), Snow and Witt (1996), and Sofia et al. (1997).

³From –17 km s⁻¹ LIC component given in Gry et al. (1995), Gry and Dupin (1997), Dupin (1998) with uncertainties assumed to be ±0.05 dex.

⁴Estimated from $n(e^-)=n(p^+)=0.1 \text{ cm}^{-3}$ and $n(H^0)=0.22 \text{ cm}^{-3}$, giving $\log N(H^0+H^+)=17.46 \text{ cm}^{-2}$.

⁵This is the denominator used to calculate the gas-phase PPM listed in columns 5 and 8 (see §5.1). Hydrogen column densities are from Table 2.

⁶The dust composition is derived from the assumption that the total elemental abundances in the cloud are given by solar abundances.

⁷The dust composition is derived from the assumption that the total elemental abundances in the cloud are given by B-star abundances.

⁸ From component 2 in York (1982). This component is predominantly neutral and is coincident with the “G” velocity vector projected in this direction if a correction of +5.6 km s⁻¹ is applied to the *Copernicus* velocity scale. This correction is required by Ca⁺ data, which find two clouds at –26±0.7 km s⁻¹ and –19.1±0.7 km s⁻¹ (Bertin et al. 1993).

⁹ $N(H^0)$ is determined directly for λ Sco (York 1983), hence PPM_g does not depend on assumed reference abundance.

¹⁰The denominator used to calculate this value is given in column 3 (with numerical values from Table 2).

¹¹The denominator used to calculate this value is given in column 3, with $\log N(H^0)=17.505 \text{ cm}^{-2}$ and $\log N(H^+)=17.15 \text{ cm}^{-2}$.

The physical conditions in the LIC are equivalent to those in the warm partially ionized medium, or intercloud medium, in the McKee and Ostriker (1977) three-phase model of the ISM. Thus, the Jones et al. (1994, 1996) results on grain destruction by interstellar shock fronts are directly applicable to the LIC conditions, and conversely the nature of the dust and gas in the LIC provides a rigorous test of these dust processing models.

B. Upstream Direction from *In Situ* Detections

The kinematic relationship between dust and gas in the LISW can be revealed by looking at the velocity dispersion of the grains measured by Galileo and Ulysses. The upstream direction and relative Sun-cloud velocity have been found from observations of interstellar He^o within the Solar System, both by direct observations of the neutral atoms with the Ulysses neutral gas experiment (Witte et al. 1996) and by observations of the backscattered He^o 584 Å radiation (e. g., Flynn et al. 1998). These directions are given in Appendix A.

The interstellar influx direction was found from *in situ* data collected with the Ulysses spacecraft, and compared with the neutral gas and backscatter results. Since the Ulysses detector has a wide field-of-view ($\pm 70^\circ$), the impact direction for individual events can not be directly determined, but is found rather from the statistical properties of the ensemble. To extrapolate from the impact direction to the upstream direction outside the heliosphere, we assume the simplest case that the particles have straight trajectories from the interstellar medium to the point where they are detected. Doing this, we neglect the grain dynamics within the Solar System. This assumption leads to an error which is smaller than the statistical error in the determination of the direction.

We apply a χ^2 -fit to the histogram of detected rotation angles with the ecliptical

longitude and latitude of the upstream direction as the parameter set. Since the line of sight of the Ulysses detector was scanning mainly latitudes (for trajectory and geometry see Grün et al. 1993), the latitude of the upstream direction is determined with higher accuracy. Figure 9 shows a contour plot of χ^2 in the two-dimensional parameter space of ecliptic coordinates.

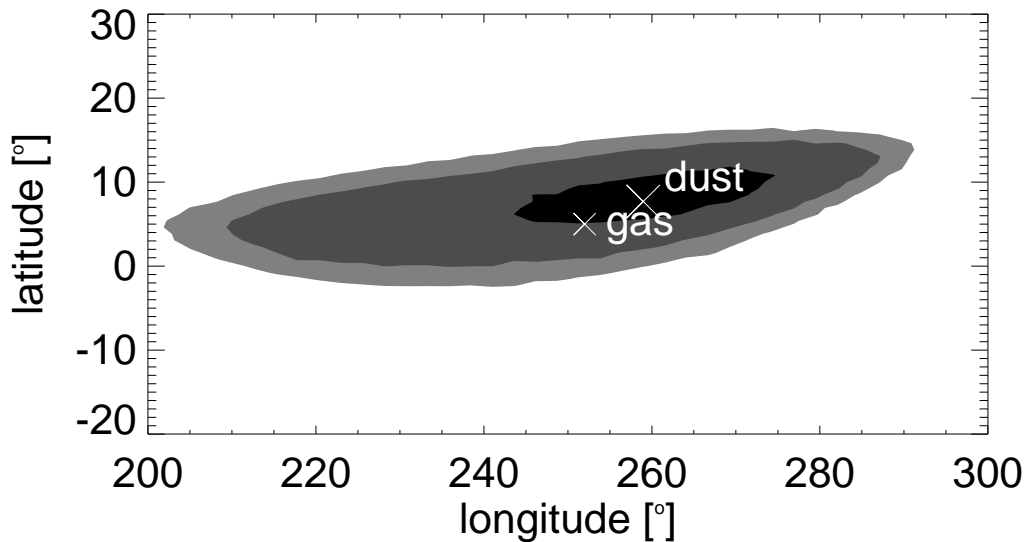


Fig. 9.— Contour plot, in ecliptic coordinates, of the upstream direction of interstellar dust grains detected by the Ulysses and Galileo satellites. Contour levels 1 σ (black), 2 σ (mid gray), and 3 σ levels (light gray) of χ^2 are shown. The parameter space is defined by ecliptic longitude (λ) and ecliptic latitude (β). The upstream direction of He $^{\circ}$ ($\lambda = 254^{\circ}$, $\beta = +5.6^{\circ}$) is shown by the “gas” label (Witte et al. 1993). The “dust” label shows the position of minimal χ^2 for the dust upstream direction ($\lambda = 259^{\circ}$, $\beta = +8^{\circ}$).

The contours shown in Figure 9 have a smaller extent in the direction of latitude than in direction of longitude and show that the latitude of the upstream direction is determined with higher accuracy. We give the upstream direction of interstellar particles as: ecliptic longitude $\lambda = 259^{\circ} \pm 20^{\circ}$, ecliptic latitude = $8^{\circ} \pm 10^{\circ}$ (1 σ -level uncertainties). The upstream direction of the interstellar gas lies inside the 1 σ -range.

C. Polarization by LISM Dust

Observations of the weak polarization ($\geq 0.05\%$) of the light of nearby ($d < 35$ pc) stars, caused by non-spherical dust grains aligned by an interstellar magnetic field in the galactic interval $l = 340^\circ \pm 70^\circ$, $b = 0^\circ \pm 40^\circ$ (Tinbergen 1982),⁴ are consistent with LISM dust grains in the size range measured by Ulysses and Galileo. The standard grain diagnostic for the size distribution of polarizing grains is the wavelength of maximum polarization (Serkowski 1973), which is not known for the LISM grains, therefore we can not make detailed predictions based on the polarization data. The LIC apparently extends only a fraction of a parsec from the Sun in this region (Lallement et al. 1995). However, the polarization strength is independent of star distance indicating that both the dust grains and magnetic field extend to the solar vicinity (Frisch 1990). We will assume that the polarizing grains in the LIC have properties consistent with the global properties for the polarizing grain population in diffuse clouds. Possibly the polarizing grains are located in the more depleted pockets of gas implied by the gas-to-dust mass ratio of λ Sco.

We obtain a minimum amount of information from the polarization data. Spatial variations in the wavelength of maximum polarization (λ_{max}) between sightlines with similar extinctions indicate that the polarizing grains are a subset of the dust grain population, with the remaining grains only contributing to the extinction (Mathis 1986), therefore we adopt the characteristics of the polarizing grains, rather than the extinguishing grains, as a model for the LIC dust. This gives a low mass cutoff in the size distribution. Mathis (1986) has calculated the size distribution for the polarizing grain populations by fitting λ_{max} , where the criteria for the size of the polarizing grain was that it be large enough to include a superparametric (SPM) cluster (which enhances the imaginary part of the

⁴This spatial interval corresponds to the upwind direction of the “local fluff” cloud complex in the local standard of rest velocity frame (Frisch 1995).

magnetic susceptibility). These relatively large polarizing grains are consistent with a deficiency of small grains seen in an MRN size distribution likely to have SPM inclusions was found to fit the observed range of $\lambda_{max}=0.35\text{--}0.72 \mu\text{m}$, providing that the small end of the size distribution was cut off at a grain radius of $a_{gr}=0.03\text{--}0.16 \mu\text{m}$. The more recent model of polarization grains of Kim and Martin (1995) also requires relatively large grains to reproduce infrared data. Thus, if models for the global properties of polarizing dust grains applies to the cloud surrounding the Solar System, then the properties of grains in nearby interstellar material in the upwind direction are consistent with the Ulysses and Galileo observations (section 3.2.2). Recently, this model has been supported by Goodman and Whittet (1995), who argue that SPM inclusions in GEMS (§6.4) have the correct sizes ($\sim 0.1\mu\text{m}$) to be the polarizing grain component.

D. LISM Abundances

D.1. LISM Abundances and Depletions

The abundances and depletions of Fe and Mg towards nearby stars are listed in Table 6. These values are based on the assumption of solar abundances. The depletion of an element X with respect to H is defined as $\delta_H = N(X)/N(H)_{observed} - N(X)/N(H)_{ref}$, where $N(X)/N(H)_{ref}$ is the reference abundance of the species X (using the standard definition). The depletions are seen to vary by ~ 0.7 dex between sightlines in the LISM if solar reference abundances are used and the comparison abundance is H^\odot . For example, solar abundances give $\delta_H(\text{Mg})=-0.44$, $\delta_H(\text{Si})=-0.25$, and $\delta_H(\text{Fe})=-0.72$. The O and N in the LIC cloud towards ϵ CMa indicate O and N are weakly depleted. These values are plotted in Figures 5 and 6.

The gas-to-dust mass ratios given in Table 2 are based on the column densities

Table 6. Depletions in Directions of Nearby Stars

HR	Star	Comp.	V km s ⁻¹	$N(\text{H}^\circ)$ cm ⁻²	$N(\text{Fe}^+)$ cm ⁻²	$\delta_{\text{H}}(\text{Fe})$ dex	$N(\text{Mg}^+)$ cm ⁻²	$\delta_{\text{H}}(\text{Mg})$ dex	Refs.
1708	α Aur	LIC	22	18.24±0.01	12.49±0.02	-1.26	12.85±0.02	-0.97	1,2
2491	α CMa	LIC	19.5	17.23 ^{+0.17} _{-0.28}	11.93±0.07	-0.98	12.20±0.08	-0.78	2,3,4
		BC	13.7	17.23±0.17	11.73±0.09	-1.01	11.95±0.05	-0.86	
2618	ϵ CMa	LIC	17	17.30 ¹¹	12.13±0.02	-0.72	12.48±0.014	-0.44	5
		BC	10	16.88 ¹¹	11.72±0.04	-0.67	12.00±0.04	-0.46	
2943	α CMi	LIC	20	17.88±0.01	12.05±0.02	-1.34	12.36±0.02	-1.1	1
		No. 2	23	17.60±0.01	11.94±0.02	-1.17	12.11±0.03	-1.07	
5191	η UMa			17.85±0.17 ⁹	12.43	-0.93	12.72	-0.71	6
5759	α Cen A	G	-18	18.0±0.02	12.45±0.02	-1.08	12.70±0.02	-0.88	2,7
5760	α Cen B	G	-18	18.0±0.02			12.72±0.08	-0.86	7
7557	α Aql	LIC	-17.4	18.26 ¹⁰	12.57±0.12		12.70±0.11		2
	GD191-B2B	LIC	21	18.27	12.48±0.18	-1.30	12.72±0.14	-1.13	2,8

The depletions are calculated with respect to H[°], in this table, using solar abundances of [Mg]=-4.42 dex and [Fe]=-4.49 dex.

¹Linsky et al. 1995

²Lallement et al. 1995

³Bertin et al. 1995

⁴Lallement et al. 1994

⁵Gry and Dupin 1997, Gry et al. 1995

⁶Frisch 1998. The uncertainties on $N(\text{Fe}^+)$ and $N(\text{Mg}^+)$ are assumed values.

⁷Linsky and Wood 1996

⁸Lemoine et al. 1996

⁹This value is determined from N[°] observations and the assumption of solar abundances (Frisch and York 1991).

¹⁰Wayne Landsman, 1997, private communication.

¹¹For solar abundances; see Tables 2, 3

presented in Table 5.

D.2. ISM towards ϵ CMa and λ Sco

Table 5 gives absorption line data for the LIC component at -17 km s^{-1} towards ϵ CMa (from Dupin 1998, Gry et al. 1995, Gry and Dupin 1996, Gry and Dupin 1998), and the LISM gas towards λ Sco (from York 1983). Note that an order of magnitude more material is found towards λ Sco than ϵ CM (Table 2). The λ Sco data are *Copernicus* data, they may sample a cluster of smaller “clouds” at closely spaced velocities. Gas-phase and dust abundances, based on both solar and B-star reference abundances for both ϵ CMa and λ Sco are presented in Table 5. Respective PPM values are calculated for these stars, where the column densities labeled “solar” and “B-star” in Table 2 are used to calculate the PPM values labeled “solar” and “B-star”, respectively. Since oxygen and nitrogen ionization are closely tied to hydrogen ionization by charge exchange, PPM values for O° and N° are calculated relative to $N(\text{H}^{\circ})$ while the PPM values listed for ions Si^+ , Mg^+ , Fe^+ , S^+ , are calculated relative to $N(\text{H}^{\circ})+N(\text{H}^+)$. Helium is not included in the PPM estimates, but represents less than a 10% correction. These enhanced abundances of refractories exhibited by the LIC are discussed in 5.3. Comparing these values to the range of Mg and Si depletions found by Fitzpatrick (1997), it is seen that the cloud around the Solar System is a weakly depleted cloud, in agreement with Frisch (1981) and GD conclusions.

The results obtained from the component 2 neutral cloud observed towards λ Sco by the *Copernicus* satellite (York 1983) are also listed in Tables 2 and 5. This component, which contains all of the neutral gas in the sightline, coincides in velocity with the LISM gas in the galactic center hemisphere (Frisch and York 1991). In this case, the assumption of B-star reference abundances is in clear disagreement with the gas-to-dust mass ratio derived from the *in situ* data.

REFERENCES

- Amari, S. & Zinner, E. 1997, in “The Astrophysical Implications of the Laboratory Study of Presolar Materials”, Eds. T.J.Bernatowicz & E.Zinner, (American Institute of Physics: Conference Proceedings), p. 287
- Amari S., Lewis, R. S., & Anders, E. 1994, GCA, 58, 471
- Anders, E., & Zinner, E. 1993, Meteoritics, 28, 490
- Aufdenberg, J. P., Hauschildt, P. H., Shore, S. N., & Baron, E. 1998, ApJ, 498, 837
- M. Baguhl, Grün, E., & Landgraf, M. 1996, in R. von Steiger, R. Lallement, & M.A.Lee, editors, *The Heliosphere in the Local Interstellar Medium*, volume 78 of *Space Science Reviews*, pages 165–172. Kluwer Academic Publishers
- Baguhl, M., Grün, E., & Landgraf, M., 1996 Space Sci. Rev., 78, 165
- Baranov, V.B., & Malama, Y.G., 1993, J. Geophys. Res., 98, 15,157
- Baranov, V.B., Izmodenov, V.V., & Malama, Y.G. 1998, J. Geophys. Res., 103, 9575
- Bernatowicz, T.J., Cowsik, R., Gibbons, P.C., Lodders, K., Fegley, Jr., B., Amari, S., & Lewis, R.S. 1996, ApJ, 472, 760
- Bertin, P., Lamers, H.J.G.L.M., Vidal-Madjar, A., Ferlet, R.& Lallement, R., 1995, A&A, 302, 899
- Bertin, P., Lallement, R., Ferlet, R., & Vidal-Madjar, A. 1993, A&A, 278, 549
- Boothroyd, A.I., Sackmann, I.-J., & Wasserburg, G.J. 1994, ApJ, 430, L77
- Bradley, J.P. 1994, Science, 265, 925
- Cardelli, J.A., & Meyer, D.M. 1997, ApJ, 477, L57

- Choi, B.-G., Huss, G.R., Wasserburg, G. J., & Gallino, R. 1998, *Science*, 282, 1284
- Clayton, D.D. 1989, *ApJ*, 340, 613
- Cox, P. 1993, in *Astronomical Infrared Spectroscopy: Future Observational Directions*, S. Kwok, A.S.P. Conf. Ser.: San Francisco, 41, 163
- Devereux, N.A., & Young, J.S. 1990, *ApJ*, 359, 42
- Diamond, C.J., Jewell, S.J., & Ponman, T.J. 1995, *MNRAS*, 274, 589
- Dorschner, J., & Henning, T. 1995, *Astron. Astrophys. Rev.*, 6, 271
- Draine 1989, *Interstellar Dust*, L.J.Allamandola & A.G.G.M. Tielens, Dordrecht: Kluwer, 313
- Draine, B.T.& Lee, H.M. 1984, *ApJ*, 285, 89
- Draine, B.T., & Salpeter, E.E. 1979, *ApJ*, 231, 77
- Dupin O., 1998, *These de Doctorat, specialite 'Astrophysique et Techniques Spatiales'*, Universite Paris 7.
- Dupuis, J., Vennes, S., Bowyer, S., Pradhan, A.K., & Thejll, P. 1995, *ApJ*, 455, 574
- Dwek, E. 1997, *ApJ*, 484, 779
- Dwek, E. 1998, *ApJ*, 501,643
- Fitzpatrick, E.L. 1997, *ApJ*, 482, L199.
- Fitzpatrick, E.L. 1996, *ApJ*, 473, L55
- Flynn, G.J. 1994, *Planet. Space Sci.*42, 1151
- Flynn, B., Vallergera, J., Dalaudier, F., & Gladstone, G.R. 1998, *J. Geophys. Res.*, 103, 648

- Frail, D.A., Weisberg, J.M., Cordes, J.M., & Mathers, C. 1994, ApJ, 436, 144
- Freivogel, P., Fulara, J., & Maier, J.P. 1994, ApJ, 431, L151
- Frisch, P. C. 1998, in preparation
- Frisch, P.C. 1998, Space Sci. Rev., 86, 107
- Frisch, P.C. 1987, astro-ph preprint No.9705231 (<http://www.xxx.lanl>)
- Frisch, P. 1996, Space Sci. Rev., 78, 213
- Frisch, P.C. 1995, Space Sci. Rev., 72, 499
- Frisch, P.C. 1990, COSPAR Colloquia Series, No.1, Physics of the Outer Heliosphere, Pergamon Press, Grzedzielski & Page (eds.), p. 19
- Frisch, P.C., & York, D.G. 1991, Extreme Ultraviolet Astronomy, Pergamon Press, Malina & Bowyer, 322
- Frisch, P.C. 1981, Nature, 293, 377
- Gayley, K.G., Zank, G.P., Pauls, H.L., Frisch, P.C., & Welty, D.E. 1997, ApJ, 487, 259
- Gehrz, R.D. 1989, Interstellar Dust, L.J.Allamandola & A.G.G.M. Tielens, Dordrecht: Kluwer, 445
- Geiss, J., Gloeckler, G., & Von Steiger, R. 1996, Space Sci. Rev., 78, 43
- Gloeckler, G., L.A. Fisk, & Geiss, J. 1997, Nature, 386, 374
- Gloeckler, G., & Geiss, J. 1997, Nature, 386, 374
- Gloeckler, G., & Geiss, J. 1998, Space Sci. Rev., 86, 127
- Goodman, A.A., & Whittet, D.C.B. 1995, ApJ, L181.

- Greenberg, J.M. 1989, in *Interstellar Dust*, L.J.Allamandola & A.G.G.M. Tielens, Dordrecht: Kluwer, 345
- Grogan, K., Dermott, S.F., & Gustafson, B.Å.S. 1996, *ApJ*, 472, 812
- Grün, E., Fechtig, H., Giese, R.H., Kissel, J., Linkert, D., Maas, D., McDonnell, J.A.M., & Morfill, G.E. 1992a, *A&AS*, 92, 411
- Grün, E., Fechtig, H., Hanner, M.S., Kissel, J., Lindblad, B.A., Linkert, D., Maas, D., Morfill, G.E., & Zook, H.A. 1992b, *Space Sci. Rev.*, 60, 317
- Grün, E., Zook, H.A., Baguhl, M., Balogh, A., Bame, S.J., Fechtig, H., Forsyth, R., Hanner, M.S., Horanyi, M., Kissel, J., Lindblad, B.A., Linkert, D., Linkert, D., Mann, I., McDonnell, J.A.M., Morfill, G.E., Phillips, J.L., Polanskey, C., Schwehm, G., Siddique, N., Staubach, P., Svestka, J., & Taylor, A. 1993, *Nature*, 362, 428
- Grün, E., Gustafson, B.Å.S., Mann, I., Baghul, M., Morfill, G.E., Staubach, P., Taylor, A., & Zook, H.A. 1994, *A&A*, 286, 915
- Grün, E., Baguhl, M., Fechtig, H., Kissel, J., Linkert, D., Linkert, G., & Riemann, R. 1995, *Planet.Space Sci.*, 43, 941
- Grün, E. & Svestka, J. 1996a, *Space Sci. Rev.*, 78, 347
- Grün, E., Baguhl, M., Riemann, R., Zook, H.A., Dermott, S., Fechtig, H., Gustafson, B.A., Hamilton, D., Hanner, M.S., Horanyi, M., Khurana, K.K., Kissel, J., Kivelson, M., Lindblad, B.A., Linkert, D., Linkert, G., Mann, I., McDonnell, J.A.M., Morfill, G.E., Polanskey, C., Schwehm, G., & Srama, R. 1996b, *Nature*, 381, 395
- Grün, E., Staubach, P., Dermott, S., Fechtig, H., Gustafson, B.Å.S., Hamilton, D.P., Hanner, M.S., Horanyi, M., Kissel, J., Lindblad, B.A., Linkert, D., Linkert, G.,

- Mann, I., McDonnell, J.A.M., Morfill, G.E., Polanskey, C.Schwehm, G., Srama, R., & Zook, H.A. 1997, Submitted to Icarus
- Gry, C., Lemonon, L., Vidal-Madjar, A., Lemoine, M., & Ferlet, R. 1995, *A&A*, 302, 497
- Gry, C., & Dupin, O. 1996, in *Science with the Hubble Space Telescope - II*, p.472, P.Benvenuti, F.D.Macchetto & E.J.Schreier, eds. Proceedings of a workshop held in Paris Dec 4-8, 1995.
- Gry, C., & Dupin, O. 1998, *A&A*, 335, 661
- Grzedzielski, S.& Lallement, R. 1996, *Space Sci. Rev.*, 78, 247
- Gustafson, B.Å.S., & Misconi, N.Y. 1979, *Nature*, 282, 276
- Gustafson, B.Å.S. 1994, *Ann. Rev. Earth & Pl. Sci.*, 22, 553
- Harris, M.J., & Lambert, D.L. 1986, *ApJ*, 285, 674
- Heiles, C. 1997, *ApJ*, 481, 193
- Heiles, C. 1998, *The Local Bubble and Beyond*, Proceedings IAU Colloquium No.166, Springer-Verlag, Eds. Dieter Breitschwerdt and Michael Freyberg Lecture Notes in Physics Series, 506, 229
- Hoppe, P., Amari, S., Zinner, E., Ireland, T., & Lewis, R.S.1994, *ApJ*, 430, 870
- Hoppe, P., Amari, S., Zinner, E., & Lewis, R.S.1995, *Geochim.Cosmochim.Acta*, 59, 4029
- Hoppe, P., Strebels, R., Eberhardt, P., Amari, S., & Lewis, R.S.1996, *Geochim.Cosmochim.Acta*, 60, 883
- Huffman, D.R. 1977, *Adv. Phys.*, 26, 129
- Huss, G.R., & Lewis, R.S. 1995, *Geochim.Cosmochim.Acta*, 59, 115

- Jewitt, D.C. & Juu, J.X. 1993, *Nature*, 392, 730
- Jewitt, D.C. & Luu, J.X. 1995, *AJ*, 109, 1867
- Jones, A.P., Tielens, A.G.G.M., & Hollenbach, D.J. 1996, *ApJ*, 469, 740
- Jones, A.P., Tielens, A.G.G.M., Hollenbach, D.J., & McKee, C.F. 1997, in “The Astrophysical Implications of the Laboratory Study of Presolar Materials”, Eds. T.J.Bernatowicz & E.Zinner, (American Institute of Physics: Conference Proceedings), p. 595
- Jones, A.P., Tielens, A.G.G.M., Hollenbach, D.J. & McKee, C.F. 1994, *ApJ*, 433, 797
- Jones, A.P., Duley, W.W., & Williams, D.A. 1990, *QJRAS*, 31, 567
- Jones, R.V., & Spitzer, L. 1967, *ApJ*, 147, 943
- Kim, K.-H., Martin, P.G., & Hendry, P.D. 1994, *ApJ*, 422, 164
- Kim, S.-H., & Martin, P.G. 1995, *ApJ*, 444, 293
- Kim, S.-H., & Martin, P.G. 1996, *ApJ*, 462, 296
- Kimura, H., & Mann, I. 1998, *ApJ*, 499, 454
- Kissel, J., Brownlee, D.E., Buchler, K., Clark, B.C., Fechtig, H., Grün, E., Hornung, K., Igenbergs, E.B., Jeßberger, E.K., Krüger, F.R., Kuczera, H., McDonnell, J.A.M., Morfill, G.M., Rahe, J., Schwehm, G.H., Sekanina, Z., Utterback, N.G., Volk, H.J., & Zook, H.A. 1986, *Nature*, 321, 336
- Krätschmer, W., & Huffman, D. R. 1979, *Astroph. & Space Sci.*, 61, 195
- Lallement, R., & Ferlet, R. 1997, *Å*, 324, 1105

- Lallement, R., Ferlet, R., Lagrange, A.M., Lemoine, M., & Vidal-Madjar, A. 1995, AA, 304, 461L
- Lallement, R., Bertin, P., Ferlet, R., Vidal-Madjar, A., & Bertaux, J.L. 1994, AA, 286, 898
- Lallement, R. 1996, Space Sci. Rev., 78, 361
- Landgraf, M., 1998, “Modeling of the Dynamics and Interpretation of the In-Situ Measurement of Interstellar Dust in the Local Vicinity of the Solar System” PhD Thesis, Ruprecht-Karls-Universitaet Heidelberg.
- Leger, A., Puget, J.M. 1984, *a*, 137, L5
- Levy, E.H., & Jokipii, J.R. 1976, Nature, 264, 423
- Lewis, R.S., Amari, S., & Anders, E. 1994, Geochim.Cosmochim.Acta, 58, 471
- Li, A., & Greenberg, J.M. 1997, A&A, 323, 566
- Linde, T.J., Gombosi, T.I., Roe, P.L., Powell, K.G., & DeZeeuw, D.L. 1997, J. Geophys. Res., 103, 1889
- Linde, T.J., PhD Thesis, University of Michigan, “Available at <http://hpcc.engin.umich.edu/CFD/publications>”
- Linsky, J.L., & Wood, B.E. 1996 ApJ, 463, 254
- Linsky, J.L., Diplas, A., Wood, B.E., Brown, A., Ayres, T.R., & Savage, B.D. 1995, ApJ, 451, 335
- Martin, P.G. 1995, ApJ, 445, L63
- Massa D., & Savage, B. in Interstellar Dust, L.J.Allamandola & A.G.G.M. Tielens, Dordrecht: Kluwer, 3

- Mathis, J.S., Rumpl, W., & Nordsieck, K.H. 1977, ApJ, 280, 425
- Mathis, J. 1986, ApJ, 308, 281
- Mathis, J. 1990, ARA&A, 28, 37
- Mathis, J. 1998, ApJ, 497, 824
- McKee, C., & Ostriker, J. 1977, ApJ, 218, 148
- Meyer, D.M., Jura, M., & Cardelli, J.A. 1998, ApJ, 493, 222
- Meyer, D.M. 1996, In “Astrophysical Implications of the Laboratory Study of Presolar Materials” 1996, AIP Conference Proceedings 402, Ed.T.Bernatowicz, E.Zinner, p.507
- Meyer, D.M., Cardelli, J.A., & Sofia, U.J. 1997, ApJ, 490, L103
- Morfill, G.E., Grün, E., & Leinert, C. 1985, The Sun and the Heliosphere in Three Dimensions, Ed. R.G.Marsden, number 123, pages 455–477. Astrophysics and Space Science Library
- Nittler, L.R., Hoppe, P., Alexander, C.M.O.D, Amari, S., Eberhardt, P., Gao, X., Lewis, R.S., Strebels, R., Walker, R.M., & Zinner, E.1995, ApJ, 453, L25
- Nittler, L.R., Alexander, C.M.O.D, Gao, X., Walker, R.M., & Zinner, E.1997, ApJ, 483, 475
- Ott, U. 1993, Nature, 364, 25
- Pauls, H.L., G.P. Zank & L.L. Williams, J. Geophys. Res., 101, 21,595, 1995.
- Pauls, H.L., & Zank, G.P. J. Geophys. Res., 102, 19,779, 1997a.
- Pauls, H.L., & Zank, G.P. 1997b, J. Geophys. Res., 102, 19,779

- Puyoo, O., & Jaffel, L. B. 1998, The Local Bubble and Beyond, Proceedings IAU Colloquium No.166, Springer–Verlag, Eds. Dieter Breitschwerdt and Michael Freyberg Lecture Notes in Physics Series, 506, 29
- Reach, W. 1988, ApJ, 335, 468
- Reach, W., Abergel, A., Boulanger, F., Desert, F.-X., Perault, M., Bernard, J.-P., Blommaert, J., Cesarsky, C., Cesarsky, D., Metcalfe, L., Puget, J.-L., Sibille, F., & Vigroux, L. 1996, A&A, 315, L381
- Roche, P.F. 1987, in Dust in the Universe, M.E. Bailey & D.A. Williams, Cambridge University Press, 415
- Rucinski, D., & Fahr, H.J.A&A, 224, 290
- Russell, S.S., Ott, U., Alexander, C.M.O'D, Zinner, E.K., & Arden, J.W. 1997, Meteoritics Planet. Sci., 32, 719
- Salama, F., & Allamandola, L. J. 1992, Nature, 358, 42
- Savage, B.D.& Sembach, K.R. 1996, ApJ470, 893
- Savage, B.D. & Sembach, K.R. 1996, ARA&A34, 279
- Serkowski, K. 1973, IAU Symp.52, Interstellar Dust and Related Topics, Eds. J.M.Greenberg & H.C. van de Hulst, Reidel, p.145
- Slavin, J.D., & Frisch, P.C. 1998, The Local Bubble and Beyond, Proceedings IAU Colloquium No.166, Springer–Verlag, Eds. Dieter Breitschwerdt and Michael Freyberg Lecture Notes in Physics Series, 506, 305
- Snow, T. P., & Witt, A. N. 1995, Science, 270, 1455

- Snow, T.P., & Witt, A.N. 1996, ApJ, 468, L65
- Sofia, U.J., Cardelli, J.A.& Guerin, K.P. 1997, ApJ, 482, L105
- Sofia, U.J., Cardelli, J.A.& Savage, B.D. 1994, ApJ, 430, 650
- Sonett, C.P., Morfill, G.E., & Jokipii, J.R. 1987, Nature, 330, 458
- Spitzer, L. 1978, Physical Processes in the Interstellar Medium, New York: Wiley
Interscience
- Taylor, A., Baggaley, W.J., & Steel, D.I. 1996, Nature, 380, 323
- Tielens, A.G.G.M., McKee, C.F., Seab, C.G., & Hollenbach, D.J. 1994,
- Tielens, A.G.G.M. 1998, ApJ, 499, 267
- Tinbergen, J., 1982, AA, 105, 53
- Travaglio, C., Gallino, R., Amari, S., Zinner, E., Woosley, S., & Lewis, R.S. 1999, ApJ, 510,
325
- Ugarte, D. 1992, Nature, 935, 707
- Vallerga, J.V., Vedder, P.W., Craig, N., & Welsh, B.Y. 1993, ApJ, 411, 729
- Vallerga, J.V. 1996, Space Sci. Rev., 78, 277
- Wallis, M.K. 1987, MNRAS, 227, 331
- Weissman, P.R. 1996, in Completing the Inventory of the Solar System, ASP conf. Proc.,
Eds. T.W. Rettig & J.M. Hahn. 107, 265
- Welty, D.E., Hobbs, L.M., Lauroesch, J.T., Morton, D.C., & York, D.G. 1995, ApJ, 449:
L135

- Welty, D.E., Morton, D.C., & Hobbs, L.M. 1996, ApJS, 106, 533
- Welty, D.E., Morton, D.C., & Hobbs, L.M. 1999, ApJ, submitted
- Whittet, D.C.B. 1992, "Dust in the Galactic Environment", London: IOP Publishing
- Witte, M., Rosenbauer, H., Banaszkiwicz, H., & Fahr, H. 1993, Advances in Space Res.,
13, (6)121
- Witte, M., Banaszkiwicz, M., & Rosenbauer, H. 1996, 1996, Space Sci. Rev., 78, 289
- Wood, B.E., & Linsky, J.L. 1997 ApJ474L, 39
- York, D.G. 1983, ApJ, 264, 172
- Zank, G.P., Pauls, H.L., Williams, L.L., & Hall, D.T. 1996, J. Geophys. Res., 101, 21639
- Zinner, E. 1997, in "The Astrophysical Implications of the Laboratory Study of Presolar
Materials", Eds. T.J.Bernatowicz & E.Zinner, (American Institute of Physics:
Conference Proceedings), 3